



HAL
open science

Is there an effect of Bay of Bengal salinity on the northern Indian Ocean climatological rainfall?

K. S. Krishnamohan, Jérôme Vialard, Matthieu Lengaigne, Sébastien Masson, Guillaume Samson, Stéphane Pous, Suresh Neetu, Fabien Durand, S. S. C. Shenoi, Gurvan Madec

► To cite this version:

K. S. Krishnamohan, Jérôme Vialard, Matthieu Lengaigne, Sébastien Masson, Guillaume Samson, et al.. Is there an effect of Bay of Bengal salinity on the northern Indian Ocean climatological rainfall?. *Deep Sea Research Part II: Topical Studies in Oceanography*, 2019, 166, pp.19-33. 10.1016/j.dsr2.2019.04.003 . hal-02301498

HAL Id: hal-02301498

<https://hal.sorbonne-universite.fr/hal-02301498v1>

Submitted on 30 Sep 2019

HAL is a multi-disciplinary open access archive for the deposit and dissemination of scientific research documents, whether they are published or not. The documents may come from teaching and research institutions in France or abroad, or from public or private research centers.

L'archive ouverte pluridisciplinaire **HAL**, est destinée au dépôt et à la diffusion de documents scientifiques de niveau recherche, publiés ou non, émanant des établissements d'enseignement et de recherche français ou étrangers, des laboratoires publics ou privés.

29
30
31
32
33
34
35
36
37
38
39
40
41
42
43
44
45
46
47
48
49

Abstract

The northern Bay of Bengal (BoB) receives a large amount of freshwater directly from monsoonal rains over the ocean, and indirectly through river runoffs. It has been proposed that the resulting strong salinity stratification inhibits vertical mixing of heat, thus contributing to maintain warm sea surface temperature and high climatological rainfall over the BoB. In the present paper, we explore this positive feedback loop by performing sensitivity experiments with a 25-km resolution regional coupled climate model, that captures the main BoB features reasonably well. We confirm that salinity stratification tends to stabilize the upper ocean, thereby increasing the mixed layer warming due to vertical mixing by $\sim +0.5^{\circ}\text{C}\cdot\text{month}^{-1}$ on annual average. Salinity however also induces a compensating cooling by altering the mixed layer heating rate by air-sea heat fluxes, so that the net effect on climatological surface temperature is negligible. During and shortly after the southwest monsoon, this compensation predominantly occurs through increased cooling by upward latent heat fluxes. During boreal winter, it occurs because salinity favours a thinner mixed layer, which is more efficiently cooled by negative air-sea heat fluxes. These compensations result in a negligible climatological surface temperature and rainfall change at all seasons. This weak influence of salinity stratification on climatological surface temperature and rainfall in our model is robust when applying a flux correction to alleviate model biases, when neglecting the solar absorption below the mixed layer and when using different atmospheric radiation and convective parameterizations.

50 1. Introduction

51 With 60% of jobs in the agriculture sector, the livelihood of the densely-populated Indian
52 subcontinent crucially depends on the Indian summer monsoon rainfall (Webster et al., 1998;
53 Gadgil and Gadgil, 2006), which accounts for about 90% of annual precipitation over India.
54 During boreal summer, the differential heating between the Asian landmass and the ocean to the
55 south sets up a low pressure area over south Asia reinforced by the elevated heating on the
56 Tibetan plateau (Li and Yanai, 1996). The dynamical response to this pressure gradient consists
57 of a low-level and large-scale cross-equatorial flow (Joseph and Raman, 1966; Findlater, 1969),
58 which induces surface evaporation and collects moisture over the Indian Ocean. From June to
59 September, the northern branch of this flow results in strong southwesterly winds over the
60 Arabian Sea (AS) and the associated moisture transport is then flushed over the Indian
61 subcontinent and Bay of Bengal (BoB) (Findlater, 1969).

62 This strong south-west monsoon rainfall and the associated larger riverine input (mainly
63 from the Ganges-Brahmaputra and Irrawaddy) results in a large freshwater input into the BoB
64 during the southwest monsoon, with rainfall accounting for more than two thirds (e.g. Sengupta
65 et al., 2006; Akhil et al., 2014; Chaitanya et al., 2014). This large freshwater input into a
66 relatively-small, semi-enclosed basin yields some of the lowest climatological Sea Surface
67 Salinities (SSS) in the tropical band (Chaitanya et al., 2014), with a maximum freshening in the
68 top 10-40 meters, resulting in a sharp near-surface salinity stratification, especially in the
69 northern BoB (e.g. Vinayachandran et al., 2002; Behara and Vinayachandran, 2016; Sengupta et
70 al., 2016). This salinity stratification has a strong stabilizing effect on the upper ocean,
71 maintaining a shallow mixed layer (Mignot et al., 2007; Girishkumar et al., 2013) and often
72 resulting in the formation of a barrier layer, i.e. a salinity-stratified layer between the bottom of
73 the mixed layer and top of the thermocline (Lukas and Lindstrom, 1991; Sprintall and Tomczak,
74 1992). Barrier layers usually appear during summer in the eastern BoB and mature during winter
75 both in amplitude and spatial extent, covering the entire northern BoB (Rao and Sivakumar,
76 2003; Thadathil et al., 2007; Kumari et al., 2018; Li et al., 2017).

77 The barrier layer impacts the mixed layer temperature heat budget, by isolating the warm
78 surface layer from the colder upper thermocline and preventing the entrainment of cold
79 subsurface water into the mixed layer (Vialard and Delecluse, 1998). The salinity stratification
80 within the barrier layer can even support temperature inversions (i.e. warmer water below than
81 within the mixed layer, e.g. Han et al., 2001; Girishkumar et al., 2013; Thadathil et al., 2016). In

82 presence of such temperature inversions, entrainment (that usually cools the mixed layer) can
83 even warm the surface layer during winter (de Boyer Montegut et al., 2007). The strong salinity
84 stratification thus appears to play a key role in maintaining a relatively high Sea Surface
85 Temperature (SST) in the BoB by reducing the vertical mixing of heat during and after the
86 southwest monsoon (de Boyer Montegut et al., 2007).

87 In a seminal study, Shenoi et al. (2002) proposed that the vertical salinity stratification in
88 BoB could contribute to a coupled ocean-atmosphere positive feedback loop that maintains
89 intense climatological rainfall regionally. In this hypothesis, summarized on the sketch of Fig. 1,
90 a strong rainfall and river freshwater forcing yields a low SSS and strong vertical salinity
91 stratification in the BoB (Step I on the Fig. 1). This strong, stable salinity stratification (and the
92 associated barrier layer) inhibits the cooling of the mixed layer by turbulent mixing at its bottom,
93 maintaining SST above 28.5°C during the entire summer monsoon (Step II on Fig. 1). Such SST
94 above 28.5°C is a necessary condition for deep atmospheric convection to occur (Gadgil et al.,
95 1984; Graham and Barnett, 1987), thus allowing to maintain regional rainfall and runoffs (Step
96 III on Fig. 1) and completing the feedback loop. Shenoi et al. (2002) supported this hypothesis by
97 the analysis of observational climatologies, that indicate that the available mixing energy from
98 the wind is not sufficient to overcome the stabilizing effect of the salinity stratification. The
99 feedback loop proposed by Shenoi et al. (2002) could thus contribute to maintain a high
100 climatological rainfall over the BoB.

101 The Shenoi et al. (2002) hypothesis is not only important to understand the present-day
102 BoB climatological rainfall, but may also be very relevant in the context of anthropogenic climate
103 change. Climate models and theoretical arguments indeed support an intensification of the
104 hydrological cycle as the troposphere warms in response to increasing greenhouse gases
105 concentrations (e.g. Held and Soden, 2006). The observational records already detect an
106 intensification of salinity contrasts as a result, *i.e.* increasing salinities in regions dominated by
107 evaporation, and decreasing salinities in high rainfall regions, including in the BoB (e.g. Durack
108 and Wijfels, 2010). The Shenoi et al. (2002) hypothesis, if correct, would provide an additional
109 positive feedback mechanism to further enhance the climate change impact on rainfall regionally
110 in the Bay of Bengal region. This provides an additional motivation to investigate the validity of
111 this hypothesis thoroughly.

112 Ocean modelling experiments have explored the consequences of the BoB salinity
113 stratification before (Han et al., 2001; Howden and Murtugudde, 2001; Behara and

114 Vinayachandran, 2016). Han et al. (2001) used a reduced-gravity ocean model and found that the
115 effect of freshwater fluxes was dominated by the effect of river runoffs and resulted in a localised
116 $\sim 0.5\text{-}1^\circ\text{C}$ surface warming in the northwestern BoB in summer, in response to the Kelvin wave
117 forced by the Ganges-Brahmaputra river inflow. Howden and Murtugudde (2001) used a reduced
118 gravity primitive equation model and only found a very local impact of river discharge on BoB
119 summer SST, confined to nearest grid points to the Ganges-Brahmaputra and Irrawady river
120 mouths, and more widespread $\sim 0.5^\circ\text{C}$ cooling in the northeastern BoB during winter. In a recent
121 study using an ocean general circulation model, Behara and Vinayachandran (2016) found that
122 freshwater fluxes induced a $\sim 0.5^\circ\text{C}$ warming in the northwestern BoB during summer, and 0.5 to
123 1.5°C cooling in the eastern BoB during both summer and winter.

124 None of the studies above however represents deep atmospheric convection explicitly, a
125 key element in the Shenoi et al. (2002) hypothesis (Fig. 1). A recent study with a coupled general
126 circulation model (Vinayachandran et al., 2015) suggests that river runoffs contribute to a 10%
127 decrease of Indian summer rainfall, opposite to what should be expected from Shenoi et al.
128 (2002) hypothesis. This study however switched off river runoffs not only in the BoB but at a
129 global scale, and finds really modest SST changes in the BoB ($\sim 0.2^\circ\text{C}$). It is therefore possible
130 that the Indian monsoon change in this study is rather associated with the remote response to
131 large SST signals in the northern Pacific and Atlantic Ocean ($>2^\circ\text{C}$). The most relevant coupled
132 model study of the Shenoi et al. (2002) hypothesis is thus that of Seo et al. (2009), using a fully
133 coupled regional circulation model. This study mimics freshwater fluxes into the BoB by
134 applying a relaxation to SSS climatology, which makes the SSS much lower in the BoB as
135 compared to their reference experiment. This increased salinity stratification however resulted in
136 a very weak salinity-induced surface warming in the northwestern BoB in summer ($\sim 0.2^\circ\text{C}$), and
137 a weak atmospheric response.

138 So far, the hypothesis of Shenoi et al. (2002) is thus not clearly supported by existing
139 numerical experiments. On the one hand, ocean modelling studies (Han et al., 2001; Howden and
140 Murtugudde, 2001; Seo et al., 2009; Behara and Vinayachandran, 2016) do not resolve potential
141 atmospheric feedbacks associated with deep atmospheric convection changes. On the other hand,
142 existing coupled model studies find rainfall changes that are either negligible (Seo et al., 2009) or
143 opposite to what is expected from the Shenoi et al. (2002) hypothesis (Vinayachandran et al.,
144 2015). For these reasons, we aim to revisit this hypothesis using a state-of-the-art regional
145 coupled model that captures the main features of the Indian Ocean mean climate, including the

146 monsoon, and its time-variability (Samson et al., 2014). We will do so by comparing reference
147 experiments with sensitivity experiments in which we neglect the influence of salinity on vertical
148 mixing (as in e.g. Vialard and Delecluse, 1998). Section 2 describes the model, the observational
149 datasets, the experimental design and the mixed layer temperature budget. Section 3 provides a
150 validation of the simulated BoB climatological features, focusing on the key processes involved
151 in Shenoi et al. (2002) hypothesis. Section 4 discusses the influence of salinity stratification on
152 BoB climate, for both summer and winter. We will also show that our results are robust
153 irrespective of whether we apply a flux correction or not to alleviate model biases, and for
154 different choices of oceanic and atmospheric parameterizations. A summary and discussion of
155 our results are finally presented in Section 5.

156

157 **2. Model and methods**

158 **2.1. Model configuration**

159 We use a regional coupled model to assess the influence of the BoB salinity stratification
160 on the northern Indian Ocean climate. This model couples the NEMO (Nucleus for European
161 Modelling of the Ocean) oceanic (Madec et al., 2008) and the WRF (Weather Research and
162 Forecasting Model) atmospheric (Skamarock and Klemp, 2008) primitive equation models
163 through the OASIS3 coupler (Valcke, 2013), and is named NOW for NEMO-OASIS-WRF.

164 We use a very similar Indian Ocean configuration to the one extensively described and
165 validated in Samson et al. (2014), and therefore only provide a brief summary of this
166 configuration in the following. This model is applied to the Indian Ocean sector (25.5°E-
167 142.25°E, 34.5°S-26°N), with the oceanic and atmospheric component sharing the same $1/4^\circ$ (~25
168 km) horizontal grid. The ocean component has 46 vertical levels, with a resolution ranging from
169 6 m to 18 m in the upper 100 m. The atmospheric component has 28 sigma vertical levels, with a
170 higher resolution of 30 m near the surface. Variable lateral boundary conditions are supplied from
171 a global simulation for the oceanic component (Brodeau et al., 2010), and from the ERA-Interim
172 reanalysis (Dee et al., 2011) for the atmosphere. River runoffs are prescribed from the Dai and
173 Trenberth (2002) climatological river product. This dataset includes the two major rivers flowing
174 into the BoB (Ganges-Brahmaputra and Irrawady that collectively represent ~80% of the total
175 river runoffs into the BoB) but also smaller rivers such as the Krishna, Godavari, and Mahanadi.

176 The ocean model parameterizations include a turbulent kinetic energy scheme for vertical
177 mixing (Blanke and Delecluse, 1993). It uses a monochromatic formulation of the penetrative
178 solar irradiance following a single exponential profile, with an e-folding depth scale set to 23 m
179 corresponding to a Type I water in Jerlov's (1968) classification (oligotrophic waters). This
180 parameterization is in line with recent observational estimates for the BoB (Lotliker et al., 2016).
181 Atmospheric model physics include the Betts-Miller-Janjic (BMJ) scheme (Janjic, 1994) for
182 subgrid-scale convection, the WRF single-moment six-class microphysics scheme WSM6 (Hong
183 and Lim, 2006), the Dudhia (1989) shortwave radiation scheme, the Rapid Radiation Transfer
184 Model (RRTM) for longwave radiation (Mlawer et al., 1997), the Yonsei University planetary
185 boundary layer (Noh et al., 2003) and the four-layer Noah land surface model (Chen et al., 1996).

186 The present model setup differs from the simulations discussed in Samson et al. (2014) as
187 the WRF model version has been updated from its version 3.2 to 3.3.1 and Dudhia (1989)
188 shortwave radiation scheme has been preferred to the one of Goddard (Chou and Suarez, 1999).
189 In line with the model version discussed in Samson et al. (2014), the reference simulation from
190 the present configuration shares a lot in common with the one presented in Samson et al. (2014).
191 Although an exhaustive validation of the present model configuration is out of the scope of this
192 paper, a validation of the main model parameters involved in the feedback loop hypothesized by
193 Shenoi et al. (2002) will be provided in Section 3.

194 **2.2. Experimental design**

195 The reference model simulation is referred to as the control run (CTL hereafter). This 18-
196 year simulation was forced at the boundaries using conditions from the 1990-2007 period. The
197 initial conditions on the 1st January 1990 are provided from ERA-Interim reanalysis data for the
198 atmospheric component and from the $\frac{1}{4}^\circ$ ocean simulation described in Brodeau et al. (2010) for
199 the ocean. Additional sensitivity experiments were performed over the same period to test the
200 impact of haline stratification on the BoB climate. They are listed in Table 1 and described
201 below.

202 Vertical mixing is parameterized using a turbulent kinetic energy closure scheme (Blanke
203 and Delecluse, 1993) in our CTL. Using a similar strategy to Vialard and Delecluse (1998) and
204 Masson et al. (2005), we conduct a "NOS" sensitivity experiment. This experiment is identical to
205 "CTL", except that the vertical mixing is resolved assuming a constant salinity of 35 pss in the
206 $[5^\circ\text{S}-25^\circ\text{N}; 65^\circ\text{E}-105^\circ\text{E}]$ region (dashed blue frame on Fig. 3d) which encompasses the BoB and
207 South-Eastern AS, where the seasonal export of BoB freshwaters induces a somewhat similar

208 behaviour to that in the BoB (e.g. de Boyer Montégut et al., 2007; Vinayachandran et al., 2007).
209 The computation of vertical mixing is smoothly transitioned to fully accounting for the effects of
210 salinity within 5° of the edges of this region. The NOS minus CTL experiment will thus
211 specifically isolate effects of the salinity stratification in the BoB region on the regional climate,
212 hence allowing to test the feedback loop hypothesized by Shenoi et al. (2002).

213 As we will see in more details in section 3, the CTL simulation strongly overestimates the
214 wind stresses over the BoB, which yields a too deep mixed layer, too thin barrier layer and
215 underestimated salinity stratification. Since the realism of the haline stratification is critical to our
216 results, we performed a wind stress-corrected reference experiment FCTL (see Table 1), in which
217 the wind stress provided to the ocean model was multiplied by a factor of 0.5 within the [8°N -
218 26°N , 76°E - 100°E] region, with a smooth transition within 6° of the edges. Penetrative solar
219 heat flux has a significant influence on the SST seasonal evolution in the BoB (e.g. de Boyer
220 Montegut et al., 2007). We will demonstrate in section 3 that this flux correction approach
221 strongly reduces the mixed layer depth (MLD) and barrier layer thickness (BLT) biases in the
222 CTL experiment, and will further present our results based on FCTL and a twin experiment that
223 neglects the effect of salinity stratification on vertical mixing (FNOS) in section 4. We will
224 demonstrate in section 4 that our results are robust irrespective of whether the flux correction is
225 applied or not.

226 Since our results could also be sensitive to some choices in physical parameterizations, we
227 have also redone twin set of experiments similar to CTL and NOS with various choices. Howden
228 and Murtugudde (2001) have shown that different SST anomalies develop in response to river
229 inputs, depending on whether solar radiation is allowed to penetrate into the ocean or not. In
230 order to test the sensitivity of our results to penetrative solar flux, we perform twin experiments
231 for CTL and NOS, where the solar penetration is disabled and the entire solar flux is absorbed
232 within the top model level (CTL_NSP and NOS_NSP experiments). Deep atmospheric
233 convection is an essential component of Shenoi et al. (2002) hypothesis, and the results presented
234 here may be sensitive to the convective scheme. The sensitivity of our results to the choice of
235 convective scheme will thus be addressed by comparing results obtained using the BMJ moist
236 convective adjustment scheme, with those obtained using the updated Kain-Fritsch (KF)
237 atmospheric convective scheme (Kain, 2004) (CTL_KF and NOS_KF experiments). Similarly,
238 the sensitivity of our results to the shortwave radiation scheme in experiments with the Goddard
239 scheme (Chou and Suarez, 1999), previously employed in Samson et al. (2014) (CTL_G and

240 NOS_G experiments). As we will see, our results on the effect of the BoB haline stratification on
 241 climatological rainfall are robust in any set of twin experiments above.

242 2.3. Mixed layer temperature budget.

243 The processes controlling SST are characterized using an online mixed layer heat budget
 244 (Vialard and Delecluse, 1998; Vialard et al., 2001). The equation for the average temperature
 245 over the time-varying mixed layer T_{ml} (a proxy for SST) reads as follows:

$$\begin{aligned}
 \partial T_{ml} = & -\frac{1}{h} \int_{-h}^0 u \partial_x T dz - \frac{1}{h} \int_{-h}^0 v \partial_y T dz - \frac{1}{h} \int_{-h}^0 D_l(T) \\
 & \text{horizontal advection} \qquad \qquad \qquad \text{lateral process} \\
 & -\frac{1}{h} (T_{ml} - T_{-h})(w_{-h} + \partial_t h) - \frac{1}{h} [K_z \partial_z T]_{-h} + \frac{Q_s(1-F_{-h}) + Q_{ns}}{\rho_0 C_p h} \qquad (1) \\
 & \text{subsurface vertical process} \qquad \qquad \qquad \text{atmospheric forcing}(F_T)
 \end{aligned}$$

247 The first two terms on the RHS respectively represent zonal and meridional temperature
 248 advection in the mixed layer, where h is the time-varying model mixed layer estimated based on a
 249 potential density increase of 0.01 kg m^{-3} relative to the density at 10-m depth and (u, v, w) are the
 250 components of the current. The second term on the RHS represents lateral mixing processes,
 251 $D_l(T)$ being model horizontal diffusion operator: this term will not be discussed in the following
 252 as it is always negligible in the present analysis. The third term on the RHS gathers the vertical
 253 exchanges of heat between the mixed layer and the subsurface ocean, including the effects of
 254 upwelling $w_{-h} (T_{-h} - T_{ml})$, entrainment $\partial_t h (T_{-h} - T_{ml})$ (computed as a residual from all the other
 255 terms) and turbulent mixing at the bottom of the mixed layer $K_z \partial_z T_{-h}$, where K_z is the vertical
 256 mixing coefficient for tracers. The last term on the RHS represents the atmospheric heat flux
 257 forcing, Q_s and Q_{ns} being respectively the solar and non-solar components of the surface heat
 258 flux, F_{-h} the fraction of incoming solar radiation that penetrates down to the depth h , ρ_0 the
 259 seawater reference density, and C_p the sea water volumic heat capacity.

260 2.4. Validation datasets

261 The model SST and rainfall climatologies distribution are validated against the Tropical
 262 Rainfall Measuring Mission (TRMM) Microwave Imager (TMI) dataset
 263 (<http://www.remss.com/tmi>). The ERA-interim dataset (Dee et al., 2011) is used to validate the
 264 wind at 10 m and air-sea heat and momentum fluxes are validated using the Tropflux product
 265 (Praveen Kumar et al., 2012, 2013).

266 The ocean model climatological salinity and temperature distributions are validated against
267 the North Indian Ocean Atlas (NIOA) (Chatterjee et al., 2012) dataset. The model MLD and BLT
268 are compared with the observationally-derived climatology of de Boyer Montégut (2004)
269 (<http://www.ifremer.fr/cerweb/deboyer/mld/home.php>). In order to be strictly comparable to this
270 product, the model MLD and isothermal layer depth (ILD, with $BLT=ILD-MLD$) are computed
271 from 5-day averaged model temperature and salinity. We use the same criteria as in de Boyer
272 Montégut (2004), i.e. a 0.2°C increase relative to 10-m depth temperature for ILD, and an
273 equivalent density increase (on average 0.065 kg m^{-3} for typical BoB temperature, salinity
274 conditions) relative to 10-m depth density for MLD. The BLT estimate is anyway robust when
275 computed with either the de Boyer Montégut (2004) criterion or the 0.01 kg.m^{-3} criterion used for
276 diagnosing the surface layer heat budget. Li et al. (2017) have found (their figure 5) that the BLT
277 climatology diagnosed from the WOA13 dataset (which is similar to the NIOA atlas we use) is
278 very similar to diagnosing this BLT from individual Argo profiles, suggesting that our approach
279 for constructing our BLT validating dataset is reasonable.

280 **3. Model validation**

281 This section provides a brief validation of the reference (CTL) and flux-corrected (FCTL)
282 simulations. The model climatology is always computed over the entire 18-years of the
283 simulations. We will validate BoB-averaged climatologies of important parameters in the Shenoi
284 et al. (2002) hypothesis, and demonstrate that the FCTL experiment compares better with
285 observations. Finally, we will show the surface mixed layer heat budget in the FCTL experiment,
286 which will allow to qualitatively check the consistency with previous studies.

287 **3.1. Testing the validity of the wind stress correction approach**

288 Fig. 2 shows the climatological seasonal cycle of several BoB-averaged parameters that are
289 important for testing Shenoi et al. (2002) hypothesis (SST, SSS, wind and wind stress, rainfall,
290 net heat flux, haline stratification measured through MLD and BLT). Observationally-derived
291 wind and wind stress are strongest during the southwest monsoon over the BoB, with a secondary
292 maximum associated with the northeast monsoon in December-January (Fig. 2a,b). Rainfall is
293 maximum in July during the southwest monsoon (Fig. 2c). Net air-sea heat fluxes into the ocean
294 are largest before the monsoon, close to zero during the southwest monsoon, and become
295 negative during the northeast monsoon (Fig. 2h). This seasonal heat flux evolution is generally
296 consistent with the evolution of SST trend. SST is indeed warmest in the BoB in April-May

297 before the southwest monsoon (Fig. 2d) and coolest in January-February during the northeast
298 monsoon. The strong monsoon rainfall (Fig. 2c) and river runoffs yield lowest salinities in
299 October right after the southwest monsoon (Fig. 2e). The MLD has a clear semi-annual cycle
300 with shallowest MLD during the inter-monsoon seasons, and deeper MLD during both monsoons
301 (Fig. 2f), due to enhanced wind stirring (in summer) and negative air-sea fluxes (in winter). The
302 barrier layer is thickest in boreal winter, i.e. after the southwest monsoon (Fig. 2g).

303 The control simulation generally reproduces the phase of the observed seasonal cycle quite
304 well, but has several marked biases. First, the model wind stress is strongly overestimated all year
305 long (by ~80% on average; see Fig. 2a). In contrast, the model wind speed is overestimated (by
306 15% on average; see Fig. 2b). However, this overestimation also combines with a 20%
307 overestimation of the wind variance (the June to September BoB-averaged CTL wind speed
308 variance is 4.5 m.s^{-1} vs. 3.7 m.s^{-1} for ERA-I). The quadratic dependence of the wind stress on the
309 wind velocity magnifies these two modest biases and results in a strong wind stress
310 overestimation over the BoB. Rainfall is also overestimated by ~55% in summer over the BoB in
311 the CTL experiment (Fig. 2c). Net heat flux into the ocean also exhibits a negative bias (Fig. 2h),
312 larger from March to October ($\sim 20 \text{ W.m}^{-2}$) mainly due an overestimated latent heat flux as a
313 consequence of the overestimated wind speed (not shown). The net heat flux bias is in line with
314 the $\sim 1^\circ\text{C}$ too cold model SST (Fig. 2d). Despite the overestimated oceanic rainfall, the SSS is too
315 salty (Fig. 2e) and the MLD too deep (Fig. 2f) all year-long in the CTL experiment. This is
316 probably because the much too strong wind stress induces too much near-surface mixing. This
317 intense wind stirring also yields a too thin barrier layer (Fig. 2g), especially in winter (the
318 January-February average BLT is $\sim 23 \text{ m}$ in CTL vs. $\sim 35 \text{ m}$ in observations). The biases discussed
319 above are of the same order or smaller than the ones in the previous coupled studies that tested
320 the Shenoi et al. (2002) hypothesis.

321 We attempted to reduce those biases by applying an ad-hoc wind stress correction in the
322 FCTL experiment. Fig. 2a shows that our strategy of the modifying wind stress is successful in
323 producing a much more realistic wind stress seasonal cycle (Fig. 2a). It also considerably
324 improves the haline stratification, confirming that the too strong wind stirring was the main cause
325 of this bias. Applying the flux correction indeed results in a strong reduction of the MLD bias all
326 through the year (Fig. 2f). It also corrects the salty SSS bias found in CTL, with SSS in FCTL
327 that even becomes fresher than observations (Fig. 2e). The barrier layer bias is also reduced, with
328 a thickness that is very close to observations in January-July and even overestimated by 5 to 10 m

329 from August to December. It must however be noted that this wind-stress correction has little
330 impact on the rainfall (Fig. 2c) and SST (Fig. 2d) systematic biases, which already suggests a
331 weak impact of salinity stratification on climatological SST and rainfall. This will be confirmed
332 by all the set of twin experiments discussed later in the paper.

333 Given that FCTL exhibits a more realistic salinity stratification (although slightly
334 overestimated) as compared to CTL, we will present results derived from this experiment in the
335 rest of section 3 and in most of section 4. We will discuss the possible effect of FCTL remaining
336 biases (too cold BoB, too strong rainfall, slightly overestimated haline stratification) on our
337 results in section 5.

338 **3.2. Winter and summer simulated climate**

339 In this subsection, we will mainly focus on summer (June to September, hereafter JJAS)
340 and winter (December to March, hereafter DJFM). Summer is the focus of Shenoi et al. (2002)
341 and is characterized by the strongest BoB freshwater forcing. We will also discuss winter, for
342 which salinity stratification impacts the BoB climate most in the only available regional coupled
343 model study (Seo et al., 2009).

344 Despite the rainfall overestimation illustrated by Fig. 2c, the FCTL experiment generally
345 reproduces the observed seasonal rainfall and wind climatologies (not shown). To quantify this,
346 we compute pattern correlations discussed hereafter which were calculated with respect to the
347 observational climatologies mentioned in section 2.4 for the northern Indian Ocean region (0° -
348 25°N ; 40°E - 100°E). This pattern correlation reaches 0.84 (summer) and 0.94 (winter) for rainfall
349 and 0.93 (summer) and 0.92 (winter) for wind speed. The FCTL simulation also captures
350 seasonal SST patterns very well (0.90 pattern correlation for summer and 0.93 for winter), despite
351 the general tendency to underestimate the SST by about $\sim 1^{\circ}\text{C}$ seen in Fig. 2d.

352 Fig. 3 provides a more thorough validation of the BoB SSS (colours) and BLT (a proxy for
353 the vertical stratification, contours). The strong freshwater fluxes arising from the summer
354 oceanic precipitation and continental runoffs result in a strong freshening (with SSS as low as 30
355 pss) in the northern and eastern part of the BoB in summer (Fig. 3a), where river runoff and
356 oceanic precipitation are most intense, with saltier waters to the south. During summer, barrier
357 layer only develops in the eastern BoB (contours on Fig. 3a). During winter, the SSS distribution
358 remains roughly consistent to that in in summer (with fresher water to the North), but with less
359 intense meridional SSS gradients (Fig. 3b). In winter, observations indicate 20 to 30 m thick
360 barrier layers develop in the northern BoB (contours on Fig. 3b) and expand into the southeastern

361 AS. The model reproduces the observed SSS patterns very well (a pattern correlation of 0.97 for
362 JJAS and 0.98 for DJMF), with low salinity in the northern and eastern BoB and saltier water to
363 the south and in the AS in both summer and winter. The model also qualitatively reproduces the
364 observed barrier layer distribution (0.80 pattern correlation in summer and 0.81 in winter), with
365 barrier layers mainly located in the eastern BoB in summer and thicker, more widespread barrier
366 layers in the south-eastern AS and BoB in winter. It must however be noted that the model BLT
367 is underestimated in the northern BoB in winter (up to 40 m in observations against 25 to 30 m in
368 the model), which could be related to the model thermohaline biases in this region, whose
369 possible impacts will be further discussed in section 5.2.

370 **3.3. Simulated seasonal upper-ocean heat balance**

371 To investigate the Shenoi et al. (2002) hypothesis with confidence, we need to assess
372 whether the upper ocean thermal heat balance (that controls the SST) is qualitatively similar in
373 our model to what was described from previous observational and modelling studies. Fig. 4
374 provides the mean seasonal cycle of the mixed layer heat budget terms (described in section 2.3)
375 averaged over the BoB, along with the MLD and surface net heat flux components.

376 From February to April, the total tendency is positive (Fig. 4a) and associated to rising SST
377 before the monsoon (Fig. 2d). This heating tendency is driven by the positive net air-sea heat
378 fluxes result from a combination of (1) increased shortwave radiation (Fig. 4b) due to the
379 northward migration of the sun during spring and low nebulosity before the monsoon and (2)
380 reduced latent heat fluxes (Fig. 4b) due to the mild winds at this time of the year (Fig. 2b). This
381 warming by the atmospheric forcing is partially counterbalanced by vertical processes (Fig. 4a),
382 which tend to cool the ocean surface by promoting mixing with deeper, cooler water. The
383 advection terms are relatively weak when averaged over the entire BoB.

384 The SST first cools slightly at the beginning of the summer monsoon (May to July, Fig.
385 2d). The initial cooling is largely the result of a strong decrease of the heating by atmospheric
386 heat fluxes (Fig. 4a), which does not balance the cooling through vertical processes any more.
387 The weaker warming by air-sea fluxes is due to both a reduction of incoming solar radiation (due
388 to the strong nebulosity) and relatively strong latent heat fluxes (Fig. 4b) associated with the
389 strong winds at this season (Fig. 2b). Towards the end of the monsoon (August to September),
390 the warming tendency due to surface net heat fluxes is almost balanced by the cooling by vertical
391 processes (Fig. 4a), and SST does not vary much in that period (Fig. 2d).

392 From October to January, the BoB cools (Fig. 2d and Fig. 4a). This cooling is driven by
393 negative surface net heat fluxes (Fig. 4b) in response to reduced incoming solar radiation due to
394 the southward migration of the sun and increased latent heat loss (Fig. 4b) due to northeast
395 monsoon winds (Fig. 2b). The longwave fluxes also contribute to the negative net heat fluxes
396 during winter months, because of a less humid atmosphere and weaker greenhouse effect. During
397 that period, the mixed layer deepens (Fig. 2f) and oceanic vertical processes act to warm the
398 surface layer and to damp the heat flux winter cooling (Fig. 4a). This warming by vertical mixing
399 and entrainment of subsurface waters is due to the presence of temperature inversion during that
400 season in the BoB in the model, as in observations (e.g. Thadatil et al., 2016).

401 This heat balance agrees qualitatively well with that presented from a forced model
402 framework in figure 3c of de Boyer Montégut et al. (2007): the BoB SST changes are flux-driven
403 with subsurface processes acting as a moderating factor. Both analyses also suggest a significant
404 role of the haline stratification in maintaining relatively high SSTs in the BoB: during winter,
405 vertical mixing and entrainment actually warm the surface layer due to the presence of a salinity-
406 sustained temperature inversion.

407

408 **4. Influence of salinity on Bay of Bengal Climatological Rainfall**

409 The analyses in section 3 suggest that the FCTL simulation captures the main
410 climatological features of the northern Indian Ocean seasonal cycle for the key parameters
411 involved in the Shenoi et al. (2002) hypothesis. The model in particular reproduces a warming
412 tendency by oceanic vertical mixing and entrainment during winter, which could not happen in
413 the absence of salinity stratification, and hence temperature inversion below the mixed layer. In
414 the following subsections, we will first investigate how salinity influences exchanges of heat
415 between the mixed layer and deeper ocean (section 4.1), before assessing its overall effect on
416 climatological SST and rainfall (section 4.2). In section 4.3, we will demonstrate that the results
417 obtained from the flux corrected experiments (FCTL and FNOS) are robust without the flux
418 correction, and with several different choices of physical parameterisations.

419 **4.1. Salinity reduces the vertical mixing of heat in the Bay of Bengal**

420 We first perform a consistency check to ascertain that the difference between FCTL and
421 FNOS experiments indeed captures the expected oceanic impact of the salinity stratification. Fig.
422 5a,c shows that the salinity stratification induces a shallower MLD everywhere in the BoB and

423 eastern AS. This salinity-induced MLD shoaling reaches 5.5 m in summer and 10.1 m in winter
424 when averaged over the BoB. In the “NOS” experiments, the MLD is only sensitive to the
425 thermal stratification, i.e. there is no barrier layer (Vialard and Delecluse, 1998). As expected, the
426 salinity-induced MLD deepening pattern matches the barrier layer thickness pattern in the FCTL
427 run, with largest ML deepening in regions where the barrier layers are thickest (contours on Fig.
428 5). The pattern correlation between FNOS-FCTL MLD difference and FCTL BLT is indeed 0.86
429 in JJAS and 0.95 in DJF. This analysis illustrates that the salinity effects assessed from FCTL
430 minus FNOS are physically consistent.

431 Upper ocean salinity stratification strengthens the upper ocean stability in the BoB and
432 eastern AS, and limits the downward mixing of heat. Fig. 5b,d shows the FCTL minus FNOS
433 climatology of the mixed layer heating rate through vertical mixing (cf. equation 1). As expected,
434 this difference is positive in regions where a barrier layer is present in FCTL. In regions where a
435 temperature inversion is present, there is a warming by vertical processes in FCTL (cf section
436 3.3), while there can only be a cooling by vertical processes in FNOS, where no temperature
437 inversions can be sustained. In regions where no temperature inversion is present, the cooling by
438 vertical processes is decreased in FCTL relative to FNOS, due to the insulating effect of the
439 barrier layer. As a result, the salinity influence on vertical mixing always favours a warming of
440 the mixed layer in regions where a barrier layer is present in FCTL (Fig. 5b,d). This salinity-
441 induced warming through vertical mixing is not, in principle, only controlled by the barrier layer
442 thickness distribution, but also by the salinity gradient across the barrier layer, temperature
443 stratification below, and wind stirring. There is however an overall reasonable correspondence
444 between the FCTL barrier layer thickness and salinity-induced change in turbulent heat fluxes at
445 the bottom of the mixed layer, especially in winter (pattern correlation of 0.47 for JJAS and 0.81
446 for DJFM).

447 Overall, the BoB salinity stratification inhibits vertical mixing, and contributes to a
448 $+0.5^{\circ}\text{C}\cdot\text{month}^{-1}$ enhancement of the mixed layer heating rate by vertical mixing during JJAS and
449 $+0.44^{\circ}\text{C}\cdot\text{month}^{-1}$ during DJFM. This impact of salinity stratification on the vertical mixing term
450 is thus consistent with the Shenoi et al. (2002) hypothesis (Step II on Fig. 1) and other previous
451 studies (de Boyer Montegut et al., 2007; Behara and Vinayachandran, 2016).

452 **4.2. Compensating effects yield a weak impact of salinity stratification on SST and**
453 **rainfall**

454 Fig. 6 quantifies the climatological differences in BoB average SST and rainfall between
 455 FNOS and FCTL. The simulated summer SST (Fig. 6a) and rainfall (Fig. 6b) climatologies are
 456 almost identical in those simulations. Maps (not shown) likewise reveal very weak local rainfall,
 457 wind and surface temperature changes, which are generally not statistically significant, including
 458 on continents. In other words, the Shenoi et al. (2002) hypothesis does not seem to operate in our
 459 model, i.e. the salinity stratification does not seem to influence the SST or rainfall climatology.
 460 As we discussed above, however, salinity stratification contributes to an anomalous $\sim 2^\circ\text{C}$ mixed
 461 layer warming through vertical mixing over the summer monsoon (i.e. $0.5^\circ\text{C}\cdot\text{month}^{-1}$ during 4
 462 months). Our simulations are thus consistent with the step II of the Shenoi et al. (2002)
 463 hypothesis on Fig. 1 (cf. Section 4.1). The absence of any significant climatological SST change
 464 however indicates that other processes compensate the salinity-induced warming through vertical
 465 mixing, yielding a weak impact on climatological SST (step III), and thus no impact on
 466 freshwater forcing through ocean-atmosphere coupling (step I). In the rest of this subsection, we
 467 will explain why there is no SST change despite the strong salinity-induced anomalous surface
 468 warming by vertical mixing.

469 Fig. 7a shows the BoB-average FCTL minus FNOS mixed layer heat budget climatology,
 470 i.e. the salinity contribution to the SST balance. In line with the analysis shown on Fig. 5c,d, the
 471 salinity stratification contributes to a mixed layer warming through vertical mixing (blue curve
 472 on Fig. 7a), in particular during and after the summer monsoon. However, this warming tendency
 473 by subsurface processes is almost entirely balanced by a cooling tendency by atmospheric forcing
 474 (orange curve on Fig. 7a). This almost equal compensation between the salinity-induced surface
 475 layer heating by vertical mixing and cooling by atmospheric forcing results in an almost nil total
 476 SST tendency (Fig. 7a) and therefore very similar SSTs in the FCTL and FNOS experiments
 477 (Fig. 6a).

478 Several processes can lead to the change in the atmospheric forcing term seen on Fig. 7a.
 479 This term reads as follows:

$$480 \quad \frac{Q_S(1-F_h)+Q_{NS}}{\rho_0 C_p h} \quad (2)$$

481 First, a change in one or several components of the surface heat flux (solar Q_S and non-solar Q_{NS}
 482 surface fluxes) can alter the net heat flux entering into the ocean and modulate the amplitude of
 483 the atmospheric forcing term. Second, a change in the MLD impacts the atmospheric forcing
 484 term by either modulating the heat capacity of the mixed layer ($\rho_0 C_p h$ at the denominator of

485 equation 2) or by regulating the fraction of solar flux that penetrates below the mixed layer (F_h in
486 equation 2). Fig. 7c allows estimating those effects separately. The red curve on Fig. 7c is an
487 offline re-computation of FCTL minus FNOS term in equation (2). It does not match exactly the
488 orange curve on Fig. 7a due to the offline computation with 5-day average rather than
489 instantaneous values, but captures its general evolution. The blue curve on Fig. 7c shows this
490 difference, but neglecting the effect of changes in surface fluxes (see Annex A for details). The
491 orange curve neglects the effects of the mixed layer heat capacity changes, and the green curve
492 those of solar penetration. When a coloured curve departs from the red curve, it indicates that
493 salinity influences the heating rate of the mixed layer through that particular effect (see Annex A
494 for details).

495 Fig. 7c shows that the influence of each of these effects is seasonally-dependent. For
496 instance, there is a clear and dominant effect of salinity on the surface forcing heating rate
497 through the mixed layer heat capacity from November to January (see yellow shading on Fig. 7c).
498 In contrast, changes of surface fluxes contribute most to the atmospheric forcing change from
499 March to October. Below, we will separately discuss the November to January (dominant effect
500 of mixed layer heat capacity) and June to October (dominant effect of changes in air-sea fluxes)
501 periods.

502 The barrier layer is thickest in the model (and observations) from November to February
503 (Fig. 2g), and this is also the season when salinity contributes to the strongest shoaling of the
504 mixed layer (Fig. 7b). Net surface heat fluxes are negative during this period (Fig. 2h) and
505 contribute to cool the oceanic mixed layer (orange curve on Fig. 4a). By making the mixed layer
506 shallower during this period, salinity reduces its heat capacity and allows a larger cooling rate in
507 response to negative surface heat fluxes. During November to January, salinity thus does not
508 change SST because the warming it induces through its effect on vertical mixing is compensated
509 by a cooling due to negative surface heat fluxes being trapped over a shallower mixed layer.

510 During June to October, the salinity-induced anomalous cooling is dominated by the effect
511 of a surface net heat flux reduction. Air-sea heat fluxes are indeed different in the FCTL and
512 FNOS experiments (Fig. 7d), with latent heat fluxes dominating those differences during this
513 period. A more detailed analysis (not shown) indicates that latent heat flux increases due to a
514 slightly warmer SST and slightly stronger surface winds in the FCTL experiment. Although those
515 mean SST and wind change are small, they are sufficient to explain the change in latent heat flux,
516 because the Clausius-Clapeyron relation implies an exponential increase of the latent heat fluxes

517 with background SST, and hence a strong sensitivity of latent heat fluxes to those variables at the
518 BoB high climatological SSTs. Overall, the slightly larger SST and winds in the FCTL
519 simulation contribute to increase upward latent heat fluxes during and shortly after the southwest
520 monsoon, largely cancelling the effect of salinity-induced warming by vertical processes.

521 **4.3. Robustness of the results**

522 Overall, the FCTL and FNOS experiments suggest that salinity stratification favours an
523 anomalous warming of the surface layer through vertical mixing, but that this warming is
524 compensated by a salinity-induced cooling of the surface layer by air-sea fluxes. As a result, the
525 SST (and consequently the rainfall) hardly changes due to salinity stratification effects in the
526 FNOS experiment. In this section, we will investigate the robustness of those results, by
527 investigating the differences in BoB SST and rainfall climatological seasonal cycle in a series of
528 twin-experiments similar to FTCL and FNOS, but no flux correction and different choices in
529 terms of physical parameterizations (cf section 2.2).

530 Fig. 8a,b shows the mean seasonal cycle of the BoB SST and rainfall in the CTL and NOS
531 experiments (i.e. as FCTL and FNOS, but without a flux correction). Although this experiment
532 has a quite different mean state to the FCTL experiment, with a saltier SSS, deeper MLD and
533 thinner BLT, there is also an almost negligible impact of salinity stratification on the BoB SST
534 and rainfall in this experiment. Fig. 8c,d shows a similar experiment to CTL (i.e. with no flux
535 correction), but where solar heat flux is not allowed to penetrate into the ocean, likewise yield
536 almost no change in climatological SST and rainfall. This illustrates that ignoring solar
537 penetration or considering it does not change the climatological SST or rainfall. Similarly,
538 sensitivity experiments similar to CTL and NOS, but with a different shortwave radiative scheme
539 (Fig. 8e,f) or convective parameterization (Fig. 8g,h) also suggest a very minor impact of the
540 haline stratification on both SST and rainfall. Overall, our coupled model results are insensitive
541 to whether or not we apply a flux correction, consider or not the penetration of solar heat flux, or
542 to a change of the parameterization of two important atmospheric physical processes in the
543 problem that we consider.

544

545 **5. Summary and discussion**

546 **5.1. Summary**

547 The monsoonal rains feed the northern BoB with a large quantity of freshwater, from
548 oceanic rain and river runoffs. This results in some of the lowest surface salinities in the tropical
549 band. Shenoi et al. (2002) proposed that the resulting very strong vertical salinity stratification is
550 involved in a positive feedback loop that sustains intense rainfall in this region. This feedback
551 loop would act as follows. The strong vertical salinity stratification inhibits the vertical mixing of
552 heat. This contributes to maintaining SST above the $\sim 28.5^{\circ}\text{C}$ threshold for deep atmospheric
553 convection, hence contributing to intense rain above the BoB, which closes the positive feedback
554 loop.

555 In the present paper, we explore the Shenoi et al. (2002) hypothesis in a 25-km resolution
556 regional coupled climate model. An 18-year long reference experiment was run and validated.
557 The model reproduces the main features of the northern Indian Ocean mean climate in both
558 summer and winter, including the warming of the surface layer through vertical mixing
559 associated with the thick barrier layer and temperature inversions during and after the monsoon.
560 It however tends to produce 50% too strong wind stress, too deep mixed layer and too thin barrier
561 layer when run without flux correction. We largely reduce those biases in a flux-corrected
562 experiment where wind stress is artificially reduced over the BoB. We will discuss possible
563 caveats associated with remaining model biases (in particular a 15% overestimation of wind
564 speed and 1°C SST cold bias over the BoB) in section 5.2.

565 The role of salinity stratification is then evaluated in a sensitivity experiment in which
566 vertical mixing is computed based on the thermal stratification only (i.e. the haline stratification
567 is neglected). Differences between the wind-stress corrected control experiment and this
568 sensitivity experiment allow evaluating the effect of salinity stratification on the northern Indian
569 Ocean mean climate. Through the analysis of the surface layer heat budget, we find that salinity
570 stratification indeed tends to warm the mixed layer through vertical mixing, during both summer
571 and winter, as hypothesized by Shenoi et al. (2002). Based on observations, Shenoi et al. (2002)
572 predicted an increase in SST and corresponding changes in precipitation related to this mixed
573 layer warming. However, in our experiments, which resolve atmospheric feedbacks, salinity
574 induces a compensating cooling through two distinct mechanisms. During early winter (from
575 November to January), this salinity-induced cooling is of oceanic origin. Salinity indeed induces
576 a thinner, lower heat-capacity mixed layer that cools more in response to the negative air-sea
577 fluxes during this season. During late summer (from July to October), the salinity-enhanced
578 cooling by surface heat-fluxes is dominated by changes in air-sea fluxes. During and shortly after

579 the southwest monsoon, salinity induces more heat losses through latent heat fluxes at the ocean
580 surface, due to slightly warmer SST and stronger winds.

581 Because of these compensating effects on the upper ocean heat budget, salinity does not
582 influence the BoB climatological SST and rainfall in our simulations. This result is very robust,
583 as it is preserved in other sets of sensitivity experiments without the flux correction; without a
584 penetration of solar heat fluxes into the ocean; and with a different parameterization of
585 atmospheric convection or shortwave fluxes. In the next subsection, we discuss our results
586 against previous studies, their robustness, and how they may be affected by model biases.

587 **5.2. Discussion**

588 Below, we will start by comparing our results with those of previous studies, for winter and
589 summer. We will then discuss caveats of the present study.

590 Let us start by comparing our results with other studies for winter. In their 4-layers
591 reduced-gravity model, Han et al. (2001) found little effect of neither rainfall nor river runoffs on
592 the winter BoB SST. Howden and Murtugudde (2001) found an overall 0.5 to 1°C cooling of the
593 Northern BoB in winter, in response to adding river runoffs, but this model has SSS biases of up
594 to 3 pss relative to the Levitus climatology in winter (their plate 2). Behara and Vinayachandran
595 (2016) also found that rivers led to an SST cooling during the entire year along the eastern and
596 northern rim of the BoB, due to winter cooling by atmospheric fluxes projecting onto a thinner
597 mixed layer. Seo et al. (2009) find a cooling over the entire northern BoB in their regional
598 coupled model in winter due to the same process. The difference between our results and those of
599 Seo et al. (2009) and Behara and Vinayachandran (2016) for winter SST arises from a different
600 balance between two competing processes. Those two studies find, as we do, that salinity reduces
601 the winter mixed layer depth, leading to a more efficient cooling by atmospheric fluxes. In
602 contrast with those two studies, we find that – as hypothesized by Shenoi et al. (2002) – salinity
603 stratification also reduces the vertical mixing of heat at the bottom of the mixed layer, with an
604 overall negligible effect on the surface layer heat budget due to this compensation. While the
605 studies by Han et al. (2001) and Howden and Murtugudde (2001) respectively suffered from a
606 very simplified modelling framework and large biases, the last three studies have comparable
607 resolutions, physical parameterizations and biases, making it difficult to conclude which one is
608 the most realistic, and calling for more studies with other coupled models.

609 For summer, Han et al. (2001) found a weak impact of both rainfall and river runoffs on
610 SST. Howden and Murtugudde (2001) found a very localised impact of the river runoff near the

611 Ganges-Brahmaputra mouth. We won't discuss Behara and Vinayachandran (2016), for which
612 the influence of river runoff on summer SST is due to changes during winter. As in our case, Seo
613 et al. (2009) found very little changes in SST and rainfall at the BoB scale during summer. We
614 find a large impact of salinity on vertical mixing of heat as in several previous studies, but with
615 little impact on SST due to a compensating change in air-sea fluxes. Except for Howden and
616 Murtugudde (2001), there is therefore overall a stronger consensus about salinity not bringing
617 any SST change in summer amongst previous studies although the underlying mechanisms may
618 be different.

619 Let us now discuss some caveats of our study. With $\frac{1}{4}$ degree grid spacing, our ocean
620 model is eddy-permitting but not eddy-resolving. This may be an issue, because the BoB has a
621 relatively strong eddy kinetic energy (EKE; e.g. Chelton et al., 2011) generated from remote
622 wind forcing and ocean internal instability (Chen et al., 2018), and eddy may contribute to the
623 SST balance through their influence on upper ocean heat transport. Comparison with altimeter
624 estimates (not shown) however indicate a reasonable representation of the EKE in the BoB, with
625 an underestimation of less than 15%.

626 Despite the fact to the model used in the present study is amongst one of the best state-of-
627 the-art coupled models for its representation of the northern Indian Ocean climate (Samson et al.,
628 2014) or when compared to the study of Seo et al. (2009), it is not exempt from biases. Even the
629 flux-corrected experiment tends to have a too low surface salinity due to too strong rainfall (Fig.
630 2c,e) and a $\sim 1^\circ\text{C}$ too cool SST all year long (Fig. 2d). Let us briefly discuss the impact of those
631 biases. As displayed on Fig. 9, the salinity stratification is overestimated in FCTL and
632 underestimated in CTL as compared to observationally-derived climatologies, yet the two
633 experiments give similar results (no impact of this salinity stratification on the climatological
634 SST and rainfall), suggesting that this bias has little impact on our results. Observed SSS
635 climatologies however generally underestimate the northern BoB freshening because of the
636 scarcity of salinity measurements in this region as suggested by the very fresh surface signals
637 reported by recent measurements from moored buoys (Sengupta et al., 2016; Wijesekera et al.,
638 2016) and satellite observations (Fournier et al., 2017). Validating the model vertical salinity
639 profile to the northernmost RAMA mooring in the BoB (15°N) indeed suggest that FCTL
640 exhibits a small surface salty bias SSS and a deeper than observed halocline (Fig. 9). Both
641 experiments also tend to underestimate the temperature stratification below ~ 50 m. These biases

642 of temperature and salinity profiles could result in an underestimation of the effect of salinity on
643 the vertical turbulent heat fluxes.

644 There is a $\sim 1^\circ\text{C}$ cold SST bias in our model setup (Fig. 2d). This bias is partly related to
645 the 15% wind speed overestimation in the BoB (Fig. 2b), which leads to an overestimated
646 evaporative cooling. This $\sim 1^\circ\text{C}$ cold bias could significantly impact our results. In observations,
647 SST is above the observed 28.5°C threshold for deep atmospheric convection (dashed line on Fig.
648 2d) from March to November, and is very close to this threshold in July-September, implying a
649 strong sensitivity to a potential small SST change. In contrast, the model is below this threshold
650 from July to March (i.e. during most of the southwest monsoon). Figure 10 compares the relation
651 between daily SST and rainfall over the BoB in the model and observations. Observed rainfall is
652 most likely at $\sim 29^\circ\text{C}$, with a large increase of strong rainfall rates occurrence between 28°C and
653 29°C . In the model, this “switch” to the convective regime occurs at lower SST, between 27 and
654 28°C . i.e. the model has a 1°C cold SST bias, but its convective threshold is also 1°C cooler than
655 in observations. For this reason, we believe that the cold bias over the BoB in the model does not
656 strongly affect our results.

657

658 **Acknowledgements**

659 The authors thank IFCPAR (Indo French Centre for Promotion of Advanced Research),
660 New Delhi for funding of the 4907-1 proposal, CNES for funding the SeaLevelALK proposal
661 and the LEFE/EC2CO program for funding of the AO2015-873251 proposal. The simulations
662 used in this study were performed on resources provided by PRACE Research Infrastructure
663 resources CURIE at TGCC, France. We also thank IRD (Institut de Recherche pour
664 le Developpement) for the financial support of the Indo-French collaboration on Indian
665 Ocean research. This is NIO contribution number XXXX.

666

667 **Annex A: processes responsible for the change in the effect of atmospheric heat fluxes**

668

669 The heating rate of the mixed layer by atmospheric heat flux forcing reads as follows:

$$\frac{Q_S(1 - \mathcal{F}_{-h}) + Q_{NS}}{\rho_0 C_P h} \quad (a)$$

670 The red curve on fig.7c shows the difference between this term in the control experiment

671 (designated by a c superscript) and “NOS” experiment (designated by a n superscript):

$$\Delta = \frac{Q_S^c(1 - \mathcal{F}_{-h^c}) + Q_{NS}^c}{\rho_0 C_P h^c} - \frac{Q_S^n(1 - \mathcal{F}_{-h^n}) + Q_{NS}^n}{\rho_0 C_P h^n} \quad (b)$$

672 This term can become large due to several processes. First, a change in one or several

673 components of the surface heat flux can alter the net heat flux entering into the ocean (solar Q_s 674 and non-solar Q_{ns} surface fluxes) and modulate the amplitude of the atmospheric forcing term.675 This effect can be evaluated by comparing Δ to the term Δ_{flux} below:

$$\Delta_{flux} = \frac{Q_S^c(1 - \mathcal{F}_{-h^c}) + Q_{NS}^c}{\rho_0 C_P h^c} - \frac{Q_S^n(1 - \mathcal{F}_{-h^n}) + Q_{NS}^n}{\rho_0 C_P h^n} \quad (c)$$

676 The computation above neglects changes in Q_S and Q_{NS} . When Δ is different from Δ_{flux} , it means

677 that the contribution of changes in fluxes matter. A similar strategy is used to identify the effects

678 of two other processes. A change in the MLD h impacts the atmospheric forcing term in two679 ways. On the one hand, it modulates the heat capacity of the mixed layer $\rho_0 C_P h$ at the

680 denominator of equation (2): a thicker mixed layer is for example less responsive to a given heat

681 flux. This effect is identified by comparing Δ to the term Δ_{hc} below:

$$\Delta_{hc} = \frac{Q_S^c(1 - \mathcal{F}_{-h^c}) + Q_{NS}^c}{\rho_0 C_P h^c} - \frac{Q_S^n(1 - \mathcal{F}_{-h^n}) + Q_{NS}^n}{\rho_0 C_P h^n} \quad (d)$$

682 On the other hand, the MLD modulates the fraction of solar flux that penetrates below the mixed

683 layer (\mathcal{F}_{-h} of last term in equation 1): a thicker mixed layer intercepts more of the incoming solar684 heat flux (i.e. $1 - \mathcal{F}_{-h}$ is larger) than a thin mixed layer. This effect is identified by comparing Δ to685 the term Δ_{sp} below:

$$\Delta_{sp} = \frac{Q_S^c(1 - \mathcal{F}_{-h^c}) + Q_{NS}^c}{\rho_0 C_P h^c} - \frac{Q_S^n(1 - \mathcal{F}_{-h^n}) + Q_{NS}^n}{\rho_0 C_P h^n} \quad (e)$$

686 Fig. 7c shows the seasonal climatology of Δ , Δ_{flux} , Δ_{hc} , and Δ_{sp} .

687 **References**

- 688 Akhil, V.P., Durand, F., Lengaigne, M., Vialard, J., Keerthi, M.G., Gopalakrishna, V.V., Deltel,
689 C., Papa, F., de Boyer Montégut, C., 2014. A modeling study of the processes of surface
690 salinity seasonal cycle in the Bay of Bengal. *J. Geophys. Res. Oceans* 119, 3926-3947.
691 doi:10.1002/2013JC009632.
- 692 Behara, A., Vinayachandran, P.N., 2016. An OGCM study of the impact of rain and river water
693 forcing on the Bay of Bengal. *J. Geophys. Res. Oceans* 121, 2425-2446.
694 doi:10.1002/2015JC011325.
- 695 Blanke, B., Delecluse, P., 1993. Variability of the tropical Atlantic Ocean simulated by a general
696 circulation model with two different mixed-layer physics. *J. Phys. Oceanogr.* 23(7), 1363-
697 1388. doi:10.1175/1520-0485(1993)023<1363:VOTTAO>2.0.CO;2.
- 698 Brodeau, L., Barnier, B., Treguier, A.M., Penduff, T., Gulev, S., 2010. An ERA40-based
699 atmospheric forcing for global ocean circulation models. *Ocean. Model.* 31(3-4), 88-104.
700 doi:10.1016/j.ocemod.2009.10.005.
- 701 Chaitanya, V.S., Lengaigne, M., Vialard, J., Gopalakrishna, V.V., Durand, F., Kranthikumar, C.,
702 Amritash, S., Suneel, V., Papa, F., Ravichandran, M., 2014. Salinity Measurements
703 Collected by Fishermen Reveal a “River in the Sea” Flowing Along the Eastern Coast of
704 India. *Bull. Am. Meteorol. Soc.* 95, 1897-1908. doi:10.1175/BAMS-D-12-00243.1.
- 705 Chatterjee, A., Shankar, D., Shenoi, SSC., Reddy, G.V., Michael, G.S., Ravichandran, M.,
706 Gopalkrishna, V.V., Rama Rao, E.P., Udaya Bhaskar, T.V.S., Sanjeevan, V.N., 2012. A
707 new atlas of temperature and salinity for the north Indian Ocean. *J. Earth. Syst. Sci.* 121(3),
708 559-593.
- 709 Chelton, D.B., Schlax, M.G., Samelson, R.M., 2011. Global observations of nonlinear mesoscale
710 eddies, *Prog. Oceanogr.*, 91, 167–216, doi:10.1016/j.pcean.2011.01.002.
- 711 Chen, F., Mitchell, K., Schaake, J., Xue, Y., Pan, H-L., Koren, V., Duan, Q.Y., Ek, M., Betts, A.,
712 1996. Modeling of land surface evaporation by four schemes and comparison with FIFE
713 observations. *J. Geophys. Res.* 101(D3), 7251-7268. doi:10.1029/95JD02165.
- 714 Chen, G., Li, Y., Xie, Q., Wang, D., 2018. Origins of eddy kinetic energy in the Bay of Bengal. *J.*
715 *Geophys. Res. Ocean.* 123, 2097-2115. <https://doi.org/10.1002/2017JC013455>
- 716 Chou, M-D., Suarez, M.J., 1999. A solar radiation parameterization (CLIRAD-SW) developed at
717 Goddard Climate and Radiation Branch for Atmospheric Studies, Goddard Space Flight
718 Center, Greenbelt, NASA Tech. Memo. NASA/TM-1999-104606(15).

- 719 Dai, A., Trenberth, K.E., 2002. Estimates of freshwater discharge from continents: Latitudinal
720 and seasonal variations. *J. Hydrometeorol.* 3, 660-687.
- 721 de Boyer Montégut, C., Madec, G., Fischer, A.S., Lazar, A., Iudicone, D., 2004. Mixed layer
722 depth over the global ocean: an examination of profile data and a profile-based climatology.
723 *J. Geophys. Res.* 109, C12003. doi:10.1029/2004JC002378.
- 724 de Boyer Montégut, C., Vialard, J., Shenoi, S.S.C., Shankar, D., Durand, F., Ethé, C., Madec, G.,
725 2007. Simulated Seasonal and Interannual Variability of the Mixed Layer Heat Budget in
726 the Northern Indian Ocean. *J. Climate* 20(13), 3249-3268. doi:10.1175/JCLI4148.1.
- 727 Dee, D.P., et al., 2011. The ERA-Interim reanalysis: Configuration and performance of the data
728 assimilation system. *Q J Roy Meteorol Soc* 137(656), 553-597. doi:10.1002/qj.828.
- 729 Dudhia, J., 1989. Numerical study of convection observed during the Winter Monsoon
730 Experiment using a mesoscale two-dimensional model. *J. Atmos. Sci.* 46, 3077-3107.
- 731 Durack, P.J., Wijffels, S.E., 2010. Fifty-year trends in global ocean salinities and their
732 relationship to broad-scale warming. *J. Climate* 23(16), 4342-4362.
- 733 Findlater, J., 1969. A major low-level air current near the Indian Ocean during the northern
734 summer. *Q. J. Roy. Meteorol. Soc.* 95, 362-380. doi: 10.1002/qj.49709540409.
- 735 Fournier, S.J., Vialard, J., Lengaigne, M., Lee, T., Gierach, M.M., Chaitanya, A.V.S., 2017.
736 Unprecedented satellite synoptic views of the Bay of Bengal “river in the sea”. *J. Geophys.*
737 *Res. Ocean*, online first, doi: 10.1002/2017JC013333.
- 738 Gadgil, S., Gadgil, S., 2006. The Indian Monsoon, GDP and Agriculture. *Economic and Political*
739 *Weekly* 41(47), 4887-4895.
- 740 Gadgil, S., Joshi, N.V., Joseph, P.V., 1984. Ocean-atmosphere coupling over monsoon regions.
741 *Nature.* 312, 141-143.
- 742 Girishkumar, M.S., Ravichandran, M., McPhaden, M.J., 2013. Temperature inversions and their
743 influence on the mixed layer heat budget during the winters of 2006–2007 and 2007–2008
744 in the Bay of Bengal. *J. Geophys. Res.* 118, 2426-2437. doi: 10.1002/jgrc.20192.
- 745 Graham, N.E., Barnett, T.P., 1987. Sea surface temperature, surface wind divergence and
746 convection over tropical oceans. *Science.* 238, 657-659. doi:10.1126/science.238.4827.657.
- 747 Han, W., McCreary, J.P., Kohler, K.E., 2001. Influence of precipitation minus evaporation and
748 Bay of Bengal rivers on dynamics, thermodynamics, and mixed layer physics in the upper
749 Indian Ocean. *J. Geophys. Res.* 106(C4),6895-6916. doi:10.1029/2000JC000403.

- 750 Held, I.M., Soden, B.J., 2006. Robust responses of the hydrological cycle to global warming. *J.*
751 *Climate* 19, 5686-5699.
- 752 Hong, S.Y., Lim, J.O.J., 2006. The WRF Single-Moment 6-Class Microphysics Scheme (WSM6)
753 *J. Korean Meteor. Soc.* 42, 129-151.
- 754 Howden, S.D., Murtugudde, R., 2001. Effects of river inputs into the Bay of Bengal. *J. Geophys.*
755 *Res.* 106(C9), 19825-19843. doi:10.1029/2000JC000656.
- 756 Janjić, Z.I., 1994. The step-mountain Eta coordinate model: Further developments of the
757 convection, viscous sublayer, and turbulence closure schemes. *Mon. Weather Rev.* 122(5),
758 927-945. doi:10.1175/1520-0493(1994)122<0927:TSMECM>2.0.CO;2.
- 759 Jerlov, N.G., 1968. *Optical oceanography*. Elsevier, London
- 760 Joseph, P.V., Raman, P.L., 1966. Existence of low level westerly jet-stream over peninsular India
761 during July. *Indian J. Meteorol. Geophys.* 17, 407-410.
- 762 Kain, J.S., 2004. The Kain-Fritsch convective parameterization: an update. *J. Appl. Meteorol.* 43,
763 170-181.
- 764 Kumari, A., Prasanna Kumar, S., Chakraborty, A., 2018. Seasonal and Interannual Variability in
765 the Barrier Layer of the Bay of Bengal. *J. Geophys. Res. Oceans* 123, 1001–1015.
766 <https://doi.org/10.1002/2017JC013213>.
- 767 Li, C., Yanai, M., 1996. The onset and interannual variability of the Asian summer monsoon in
768 relation to land-sea thermal contrast. *J. Climate* 9, 358-375.
- 769 Li, Y., Han, W., Ravichandran, M., Wang, W., Shinoda, T., Lee, T., 2017. Bay of Bengal salinity
770 stratification and Indian summer monsoon intraseasonal oscillation: 1. Intraseasonal
771 variability and causes, *J. Geophys. Res. Oceans* 122, 4291-4311, doi:
772 10.1002/2017JC012691.
- 773 Lotliker, A.A., Omand, M.M., Lucas, A.J., Laney, S.R., Mahadevan, A., Ravichandran, M.,
774 2016. Penetrative radiative flux in the Bay of Bengal. *Oceanography* 29, 214-221.
- 775 Lukas, R., Lindstrom, E., 1991. The mixed layer of the western equatorial Pacific Ocean *J.*
776 *Geophys. Res.* 96(S01), 3343-3357. doi:10.1029/90JC01951.
- 777 Madec, G., 2008. NEMO ocean engine, Note du Pôle de modélisation, Institut Pierre-Simon
778 Laplace (IPSL), France, No 27, ISSN No 1288-1619, 2008.
- 779 Masson, S., et al., 2005. Impact of barrier layer on winter–spring variability of the southeastern
780 Arabian Sea. *Geophys. Res. Lett.* 32, L07703. doi:10.1029/2004GL021980p.

- 781 Mignot, J., de Boyer Montégut, C., Lazar, A., Cravatte, S., 2007. Control of salinity on the mixed
782 layer depth in the world ocean: 2. Tropical areas, *J. Geophys. Res.* 112, C10010.
783 doi:10.1029/2006JC003954.
- 784 Mlawer, E.J., Taubman, S.J., Brown, P.D., Iacono, M.J., Clough, S.A., 1997. Radiative transfer
785 for inhomogeneous atmospheres: RRTM, a validated correlated-k model for the longwave,
786 *J. Geophys. Res.* 102(D14), 16663-16682. doi:10.1029/97JD00237.
- 787 Noh, Y., Cheon, W.G., Hong, S.Y., Raasch, S., 2003. Improvement of the K-profile model for
788 the planetary boundary layer based on large eddy simulation data. *Bound. Lay. Meteorol.*
789 107(2), 401-427. doi:10.1023/A:1022146015946.
- 790 Praveen Kumar, B., Vialard, J., Lengaigne, M., Murty, V., McPhaden, M., 2012. Tropflux: air-
791 sea fluxes for the global tropical oceans—description and evaluation. *Clim. Dyn.* 38, 1521-
792 1543. doi:10.1007/s00382-011-1115-0.
- 793 Praveen Kumar, B., Vialard, J., Lengaigne, M., Murty, V., McPhaden, M., Cronin, M., Pinsard,
794 F., Reddy, K.G., 2013. Tropflux wind stresses over the tropical oceans: Evaluation and
795 comparison with other products. *Clim. Dyn.* 40, 2049. <https://doi.org/10.1007/s00382-012-1455-4>.
- 797 Rao, R.R., Sivakumar, R., 2003. Seasonal variability of sea surface salinity and salt budget of the
798 mixed layer of the north Indian Ocean, *J. Geophys. Res.* 108(C1), 3009.
799 doi:10.1029/2001JC000907.
- 800 Samson, G., Masson, S., Lengaigne, M., Keerthi, M.G., Vialard, J., Pous, S., Madec, G.,
801 Jourdain, N.C., Jullien, S., Menkes, C., Marchesiello, P., 2014. The NOW regional coupled
802 model: Application to the tropical Indian Ocean climate and tropical cyclone activity. *J.*
803 *Adv. Model. Earth Syst.* 6, 700-722. doi:10.1002/2014MS000324.
- 804 Sengupta, D., Bharath Raj, G.N., Shenoi, S.S.C., 2006. Surface freshwater from Bay of Bengal
805 runoff and Indonesian throughflow in the tropical Indian Ocean. *Geophys. Res. Lett.* 33,
806 L22609. doi:10.1029/2006GL027573.
- 807 Sengupta, D., Bharath Raj, N., Ravichandran, M., Sree Lekha, J., Papa, F., 2016. Near-surface
808 salinity and stratification in the north Bay of Bengal from moored observations. *Geophys.*
809 *Res. Lett.* 43, 4448-4456. doi:10.1002/2016GL068339.
- 810 Seo, H., Xie, S., Murtugudde, R., Jochum, M., Miller, A.J., 2009. Seasonal effects of Indian
811 Ocean freshwater forcing in a regional coupled model. *J. Climate* 22, 6577-6596.

- 812 Shenoi, S.S.C., Shankar, D., Shetye, S.R., 2002. Differences in heat budgets of the near-surface
813 Arabian Sea and Bay of Bengal: Implications for the summer monsoon. *J. Geophys. Res.*
814 107(C6), 1-14.
- 815 Skamarock, W.C., Klemp, J.B., 2008. A Time-Split Nonhydrostatic Atmospheric Model for
816 Weather and Forecasting Applications. *J. Comp. Phys.* 227, 3465-3485,
817 doi:10.1016/j.jcp.2007.01.037.
- 818 Sprintall, J., Tomczak, M., 1992. Evidence of the barrier layer in the surface layer of the tropics,
819 *J. Geophys. Res.* 97(C5), 7305-7316.
- 820 Thadathil, P., Muraleedharan, P.M., Rao, R.R., Somayajulu, Y.K., Reddy, G.V.,
821 Revichandran, C., 2007. Observed seasonal variability of barrier layer in the Bay of
822 Bengal, *J. Geophys. Res.* 112, C02009, doi:10.1029/2006JC003651.
- 823 Thadathil, P., Suresh, I., Gautham, S., Prasanna Kumar, S., Lengaigne, M., Rao, R.R., Neetu, S.,
824 Hegde, A., 2016. Surface layer temperature inversion in the Bay of Bengal: Main
825 characteristics and related mechanisms. *J. Geophys. Res. Oceans* 121, 5682-5696,
826 doi:10.1002/2016JC011674.
- 827 Valcke, S., 2013. The OASIS3 coupler: A European climate modelling community software,
828 *Geosci. Model. Dev.* 6(2), 373-388, doi:10.5194/gmd-6-373-2013.
- 829 Vialard, J., Delecluse, P., 1998. An OGCM Study for the TOGA Decade. Part I: Role of Salinity
830 in the Physics of the Western Pacific Fresh Pool. *J. Phys. Oceanogr.* 28(6), 1071-1088.
831 doi:10.1175/1520-0485(1998)028<1071:AOSFTT>2.0.CO;2.
- 832 Vialard, J., Menkes, C., Boulanger J.P., Delecluse P., Guilyardi, E., McPhaden, M.J., Madec, G.,
833 2001. A model study of oceanic mechanisms affecting equatorial Pacific sea surface
834 temperature during the 1997-98 El Niño. *J. Phys. Oceanogr.* 31(7), 1649-1675.
- 835 Vinayachandran, P.N., Jahfer, S., Nanjundiah, R.S., 2015. Impact of river runoff into the ocean
836 on Indian summer monsoon. *Environ. Res. Lett.* 10(5), 054008. doi:10.1088/1748-
837 9326/10/5/054008.
- 838 Vinayachandran, P.N., Murty, V.S.N., Ramesh Babu, V., 2002. Observations of barrier layer
839 formation in the Bay of Bengal during summer monsoon. *J. Geophys. Res.* 107(C12), 8018,
840 doi:10.1029/2001JC000831.
- 841 Vinayachandran, P.N., Shankar, D., Kurian, J., Durand, F., Shenoi, S.S.C., 2007. Arabian Sea
842 mini warm pool and the monsoon onset vortex. *Current Sci.* 93(2), 203-214.
- 843 Webster, P.J., Magana, V.O., Palmer, T.N., Shukla, J., Tomas, R.A., Yanai, M., Yasunari, T.,

844 1998. Monsoons: Processes, predictability and prospects for prediction. *J. Geophys. Res.*
845 103 (C7), 14451-14510.

846 Wijesekera, H.W., et al., (2016) ASIRI: an ocean–atmosphere initiative for Bay of Bengal. *Bull.*
847 *Am. Meteorol. Soc.* 97(10), 1859-1884.

848

849

850

851

ACCEPTED MANUSCRIPT

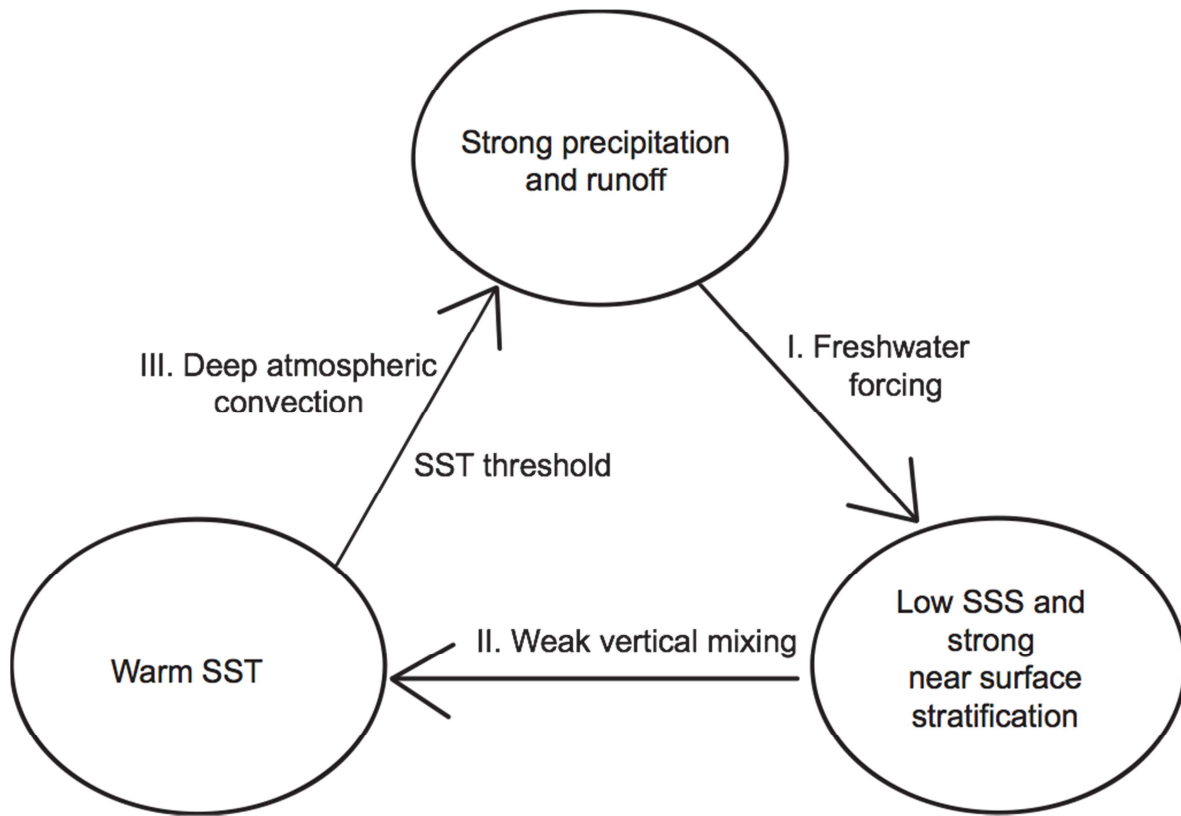
852
853
854

Experiment name	Purpose
CTL	Reference experiment. See text for details on resolution & configuration.
NOS	As CTL but with no impact of salinity on vertical mixing.
FCTL	As CTL, but with wind stress correction over the Bay of Bengal.
FNOS	As FCTL, but with no impact of salinity on vertical mixing.
CTL-NSP	As CTL, but with no solar flux penetration into the ocean.
NOS-NSP	As CTL_NSP, but with no impact of salinity on vertical mixing.
CTL-G	As CTL, but using Goddard shortwave radiation scheme.
NOS-G	As NOS, but using Goddard shortwave radiation scheme.
CTL-KF	As CTL, but using Kain-Fritsch sub-grid atmospheric convection scheme.
NOS-KF	As NOS, but using Kain-Fritsch sub-grid atmospheric convection scheme.

855

856 **Table 1:** NOW (NEMO-Oasis-WRF) regional coupled model experiments used in this study.

857
858
859
860

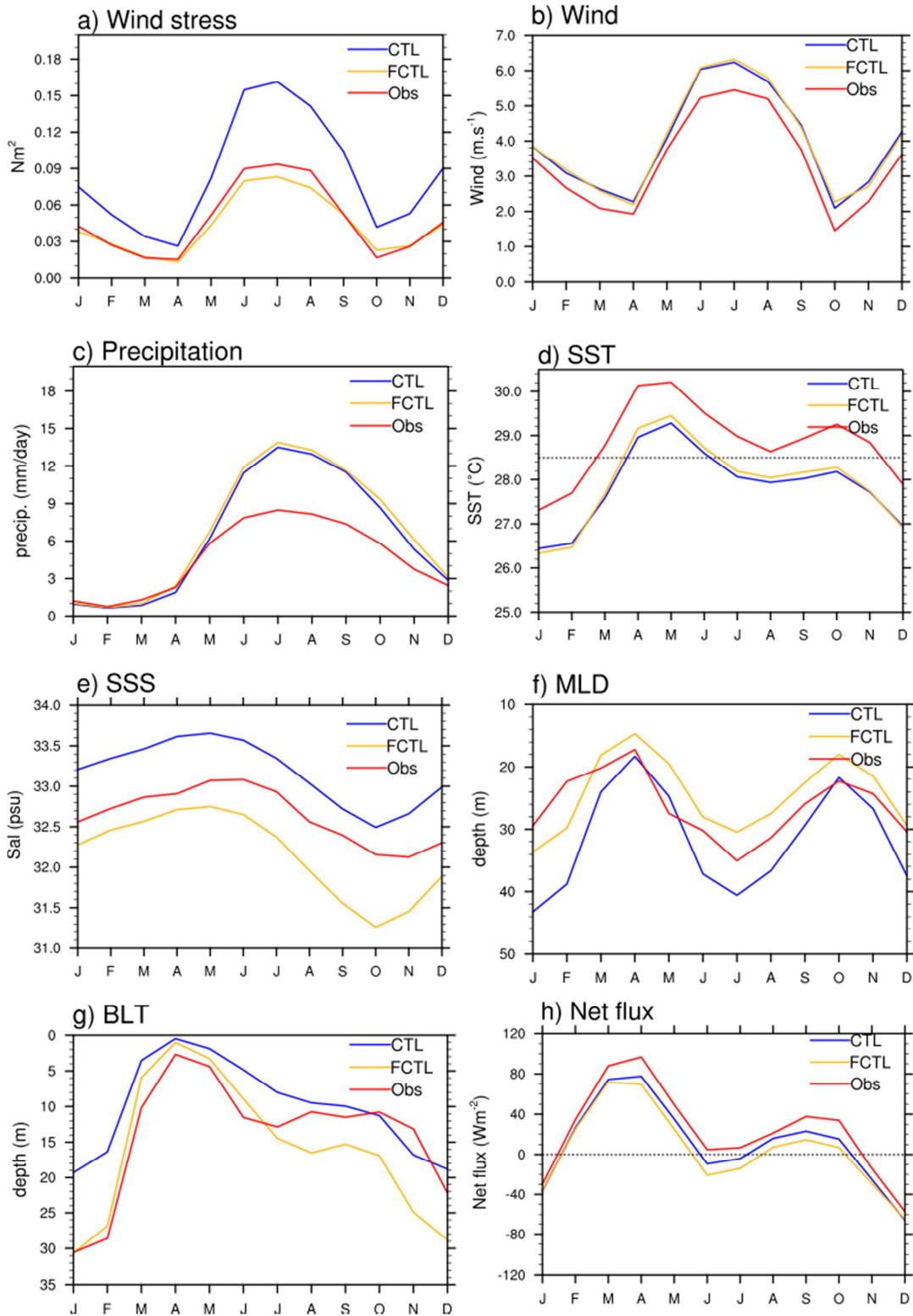


861

862 **Figure 1:** Sketch of the positive feedback mechanism proposed by Shenoi et al. (2002), by which
863 the BoB haline stratification could sustain enhanced regional precipitation.

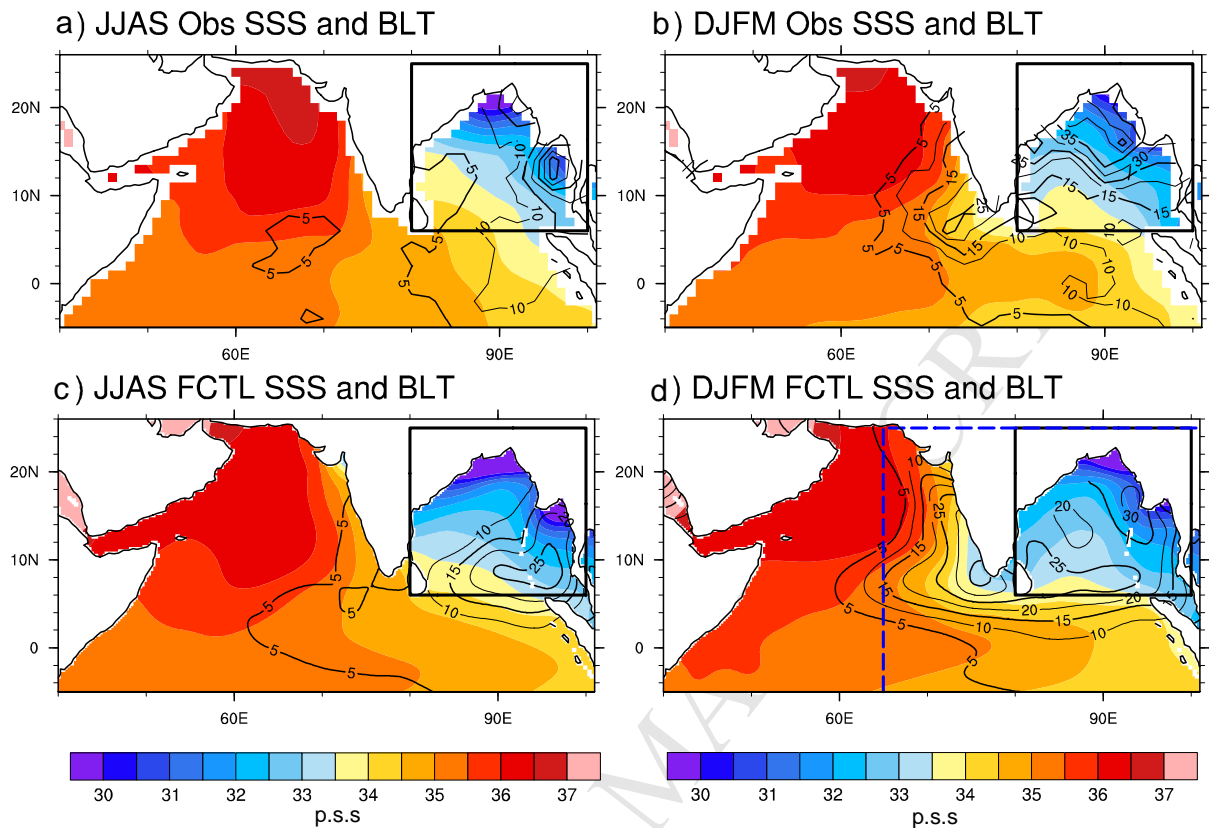
864

865



867 **Fig. 2** Averaged BoB (6°N-25°N, 80°E-100°E, see region on Fig. 3) climatological seasonal
868 cycle for CTL (Blue) & FCTL (flux correction applied on wind stress: see text for details,
869 yellow) experiments and observations (red) for (a) wind stress (N.m^{-2}), (b) wind speed (m.s^{-1}) (c)
870 precipitation (mm.day^{-1}) (W.m^{-2}), (d) Sea Surface Temperature (SST, °C), (e) Sea Surface
871 Salinity (SSS, pss), (f) mixed layer depth (MLD, m) (g) Barrier Layer Thickness (BLT, m) and
872 (h) net heat flux. Observed climatologies are obtained from the TropFlux 1990-2007 average for
873 wind stress and net heat flux, ERA-interim 1990-2007 average for wind speed, TMI 1998-2006
874 average for SST, TRMM 1998-2011 average for rainfall, NIOA climatology for SSS and de
875 Boyer Montegut et al. (2004) climatology for MLD and BLT. The dashed horizontal line on
876 panel d indicates the observed threshold (28.5°C) for deep atmospheric convection.

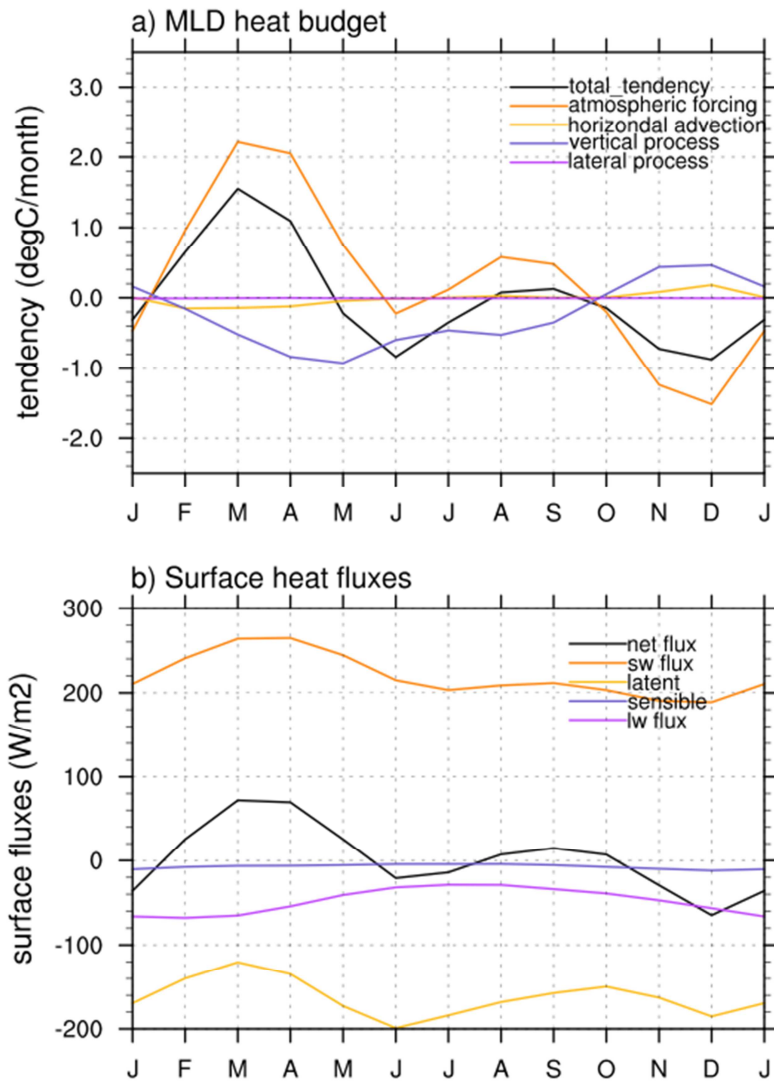
877



878

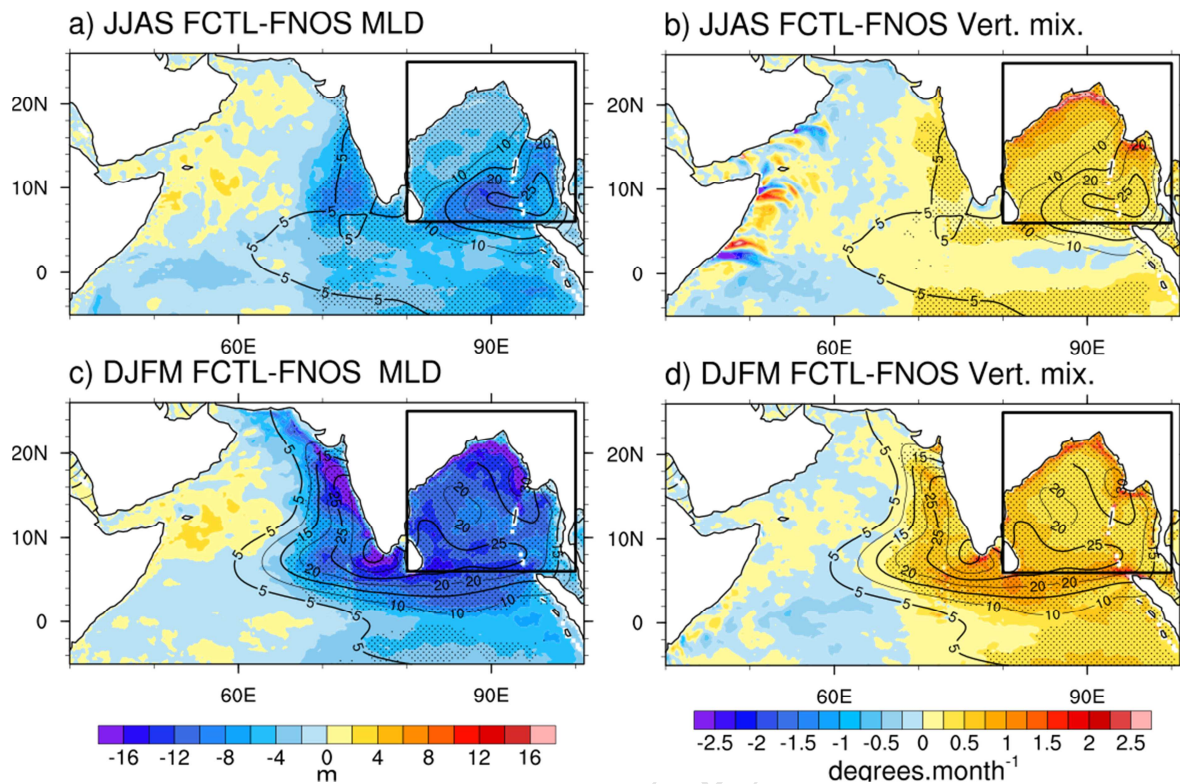
879 **Fig. 3** Summer (June to September: JJAS) (**left**) and Winter (December to March; DJFM) (**right**)
 880 climatologies of observation (**top**) and FCTL (**bottom**) Sea Surface Salinity (SSS, shading, pss)
 881 and Barrier Layer Thickness (BLT, contours, meters). For the model data, a horizontal smoothing
 882 has been applied, with a similar spatial scale than that used for the observationally-derived
 883 climatologies i.e. with a smoothing radius of 175 km for BLT as for de Boyer Montegut et al.
 884 (2004) and 4° (444 km) for SSS as for the NIOA climatology. The dashed blue frame on panel d
 885 indicates the region over which the influence of salinity on vertical mixing is neglected in the
 886 series of “NOS” experiments (see table 1).

887



888

889 **Figure 4.** Averaged BoB climatological seasonal cycle of FCTL (a) mixed layer heat budget
 890 terms ($^{\circ}\text{C}\cdot\text{month}^{-1}$, see section 2.3 for details) and (b) surface net heat fluxes and its four
 891 components ($\text{W}\cdot\text{m}^{-2}$).

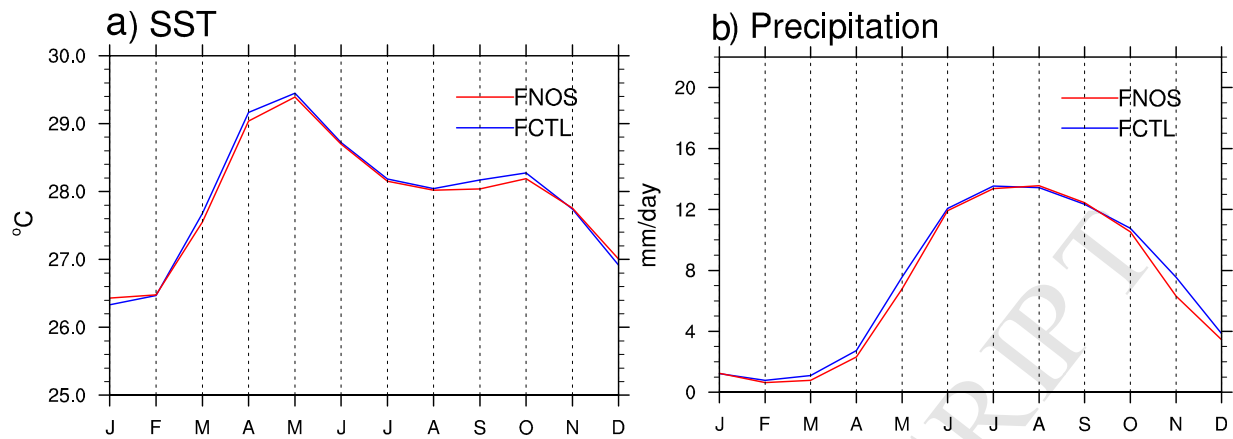


892

893 **Figure 5.** (Top) Summer (JJAS) and (bottom) winter (DJFM) climatological maps of FCTL
 894 minus FNOS (left) mixed layer depth (m) and (right) vertical mixing term of the mixed layer
 895 heat budget ($^{\circ}\text{C}\cdot\text{month}^{-1}$). The FCTL run climatological barrier layer thickness is overlaid as
 896 contours. Dots indicate regions for which MLD (left) and vertical mixing (right) differences
 897 between the FCTL and FNOS simulations are significantly different from zero at the 95%
 898 confidence level (using a one-tailed student's t-test with degrees of freedom equal to number of
 899 years minus one).

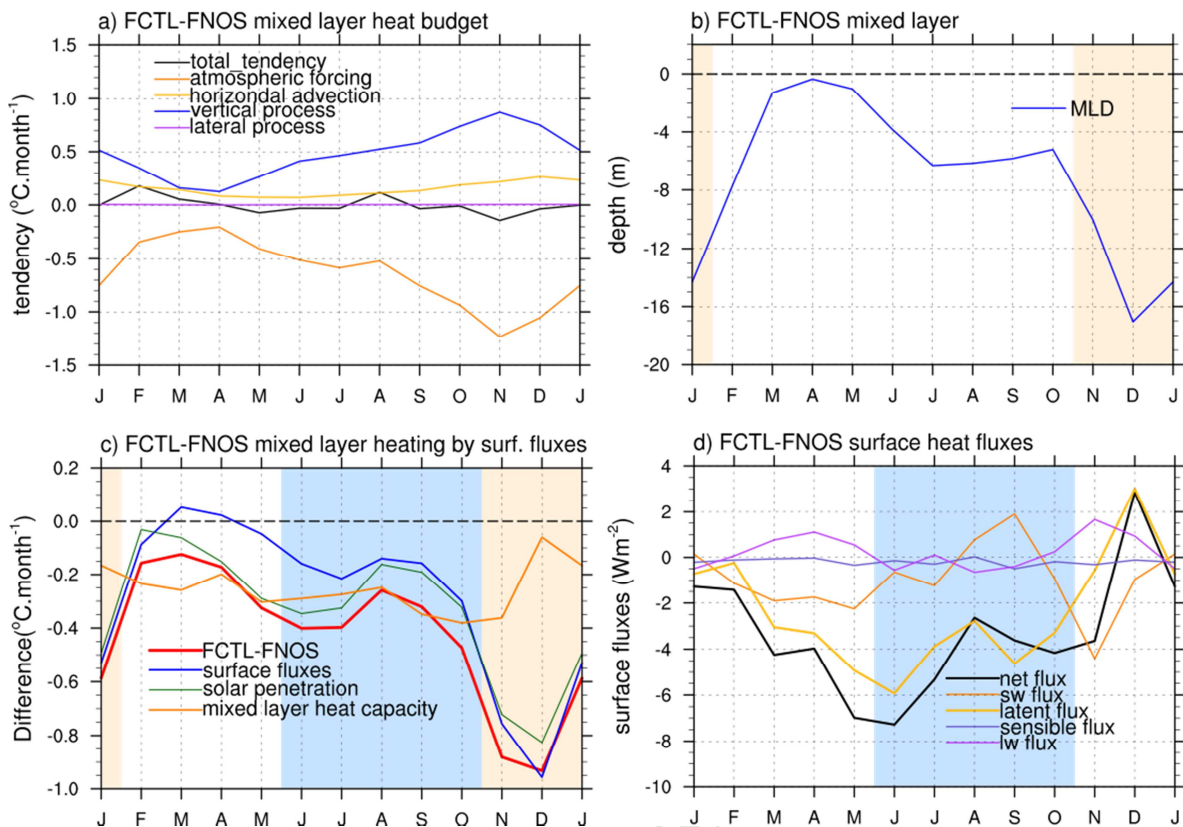
900

901



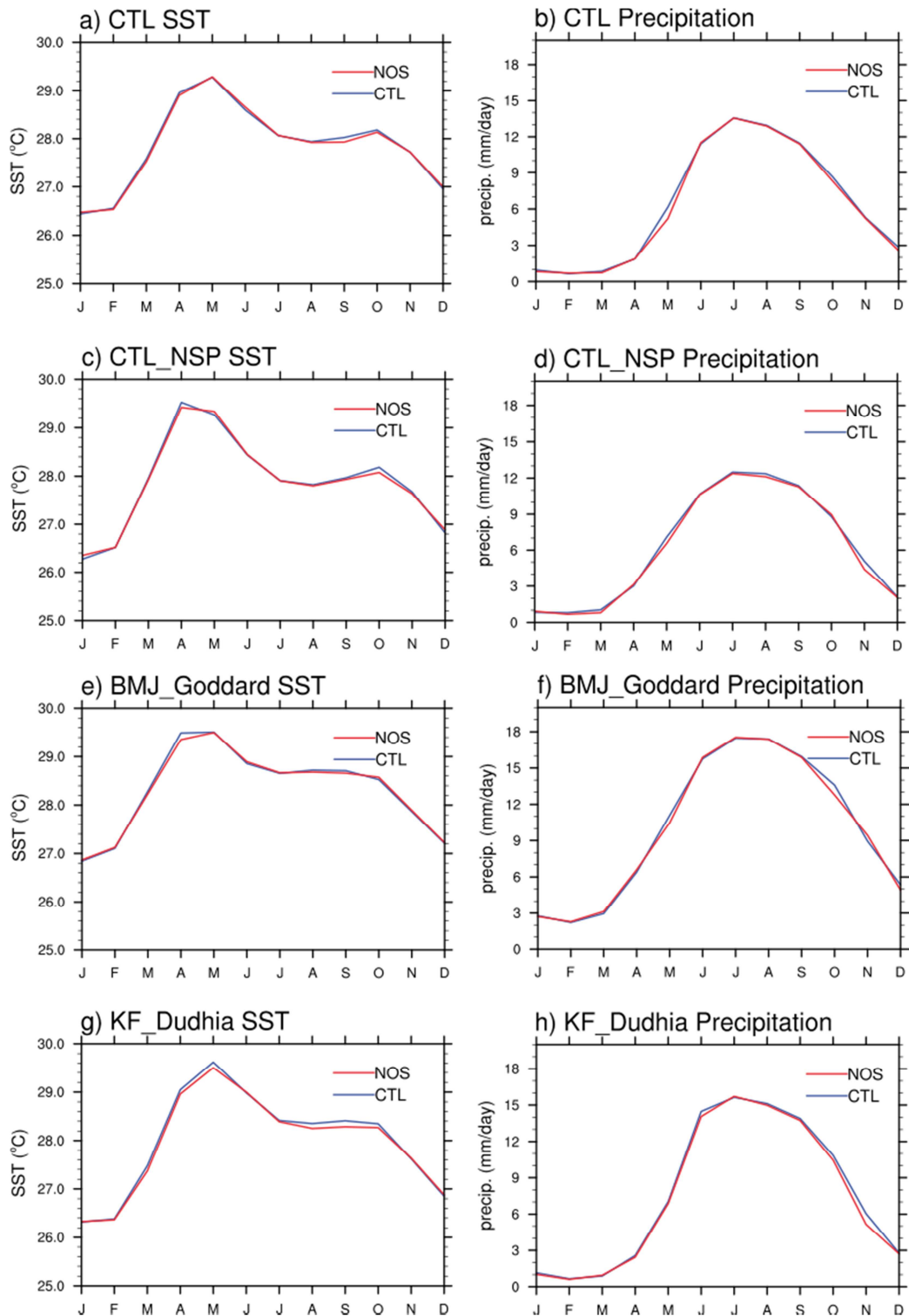
902

903 **Figure 6.** Average BoB FCTL and FNOS (e) SST and (f) precipitation climatological seasonal
904 cycle.



905

906 **Figure 7.** Average BoB climatological seasonal cycle of FCTL minus FNOS (a) MLD heat
 907 budget ($^{\circ}\text{C}\cdot\text{month}^{-1}$), (b) MLD (m) and (d) surface fluxes ($\text{W}\cdot\text{m}^{-2}$). (c) shows the FCTL minus
 908 FNOS recomputed atmospheric forcing term (thick red curve). The green curve allows to
 909 evaluate the effect of solar penetration, the blue curve the effect of the change in surface heat
 910 fluxes and the orange one the effect of the changes in mixed layer heat capacity (see text and
 911 Annex A for details). The blue shading highlights the July to October period and the salmon
 912 shading highlights the November to January period.

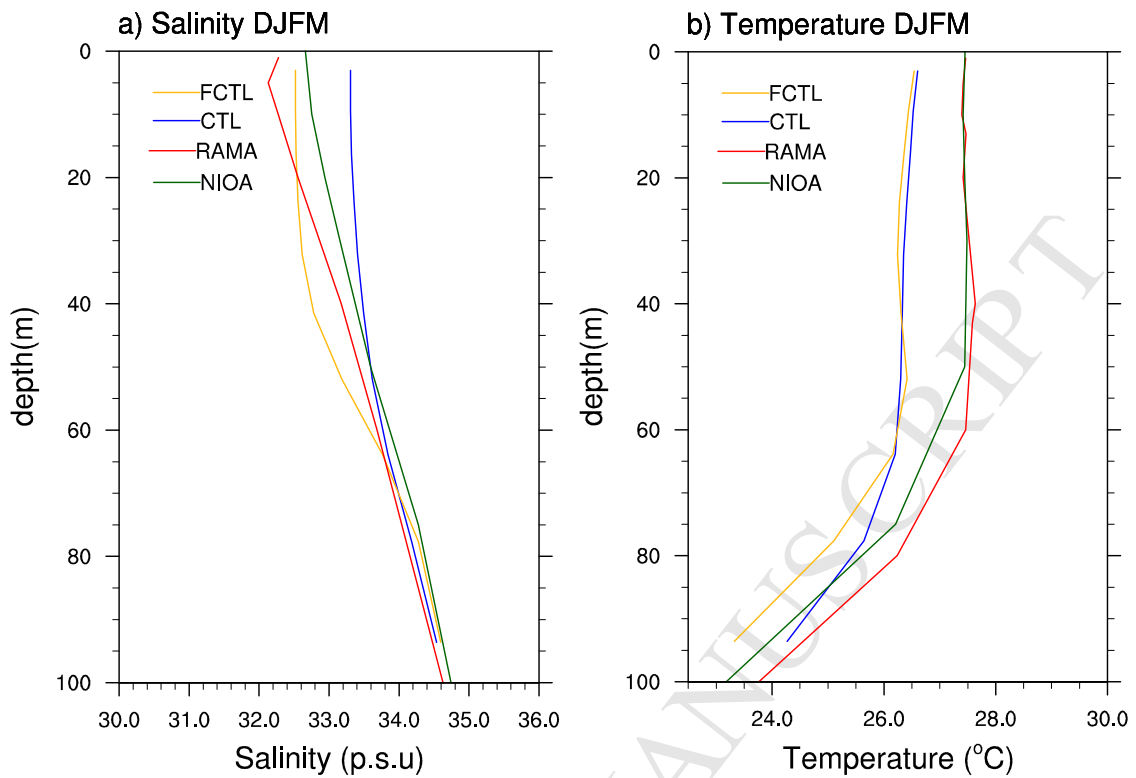


913

914 **Fig. 8:** Averaged BoB CTL and NOS mean seasonal cycle of (a) SST and (b) precipitation (i.e.
 915 same as 8ef but without flux corrections). (c)-(d) Same as (a)-(b), but for CTL-NSP and NOS-
 916 NSP (i.e. with the penetration of solar radiation into the ocean de-activated). (e)-(f) Same as (a)-

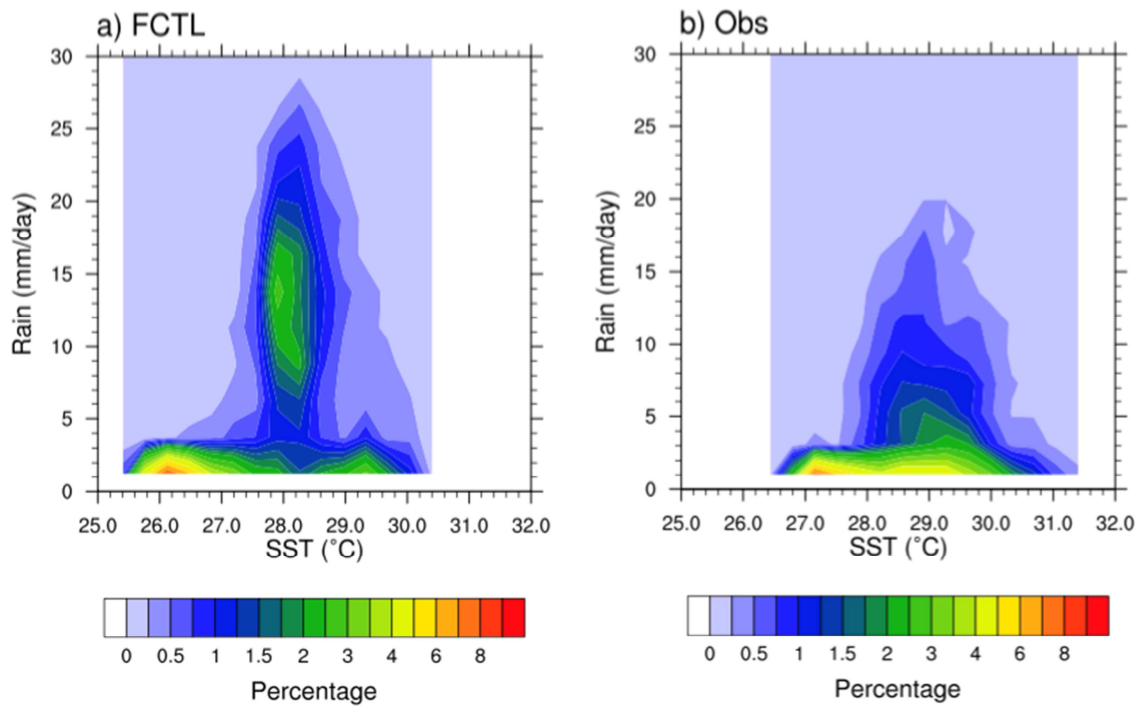
- 917 **(b)**, but for CTL-G and NOS-G (Goddard shortwave radiation parameterization). **(g)-(h)** Same as
918 **(a)-(b)**, but for CTL-KF and NOS-KF (Kain-Fritsch convective parameterization).

ACCEPTED MANUSCRIPT



919

920 **Fig 9.** Winter (DJFM) temperature and salinity BoB-averaged climatological profiles for
921 longitude 90°E and latitude 15°N from the RAMA buoy (red), NIOA product (green), CTL (blue)
922 and FCTL (yellow).



923

924 **Figure 10:** SST-rainfall relation in (a) the FCTL simulation and (b) from TMI and TRMM
 925 observations. The probability density function (%) was constructed from daily SST and rainfall
 926 over the BoB region, using $2.5 \text{ mm}\cdot\text{day}^{-1}$ and 0.33°C wide bins.